Compression-Activated Thermally Enhanced Liquid Metal Composites with Tunable Functional Properties

by

Aastha Uppal

A Dissertation Presented in Partial Fulfillment
of the Requirements for the Degree
Doctor of Philosophy

Approved September 2022 by the
Graduate Supervisory Committee:

Konrad Rykaczewski, Co-Chair
Robert Y. Wang, Co-Chair
Beomjin Kwon
Gaurang Choksi
Patrick Phelan

ARIZONA STATE UNIVERSITY

December 2022

ABSTRACT

Thermal management of electronics is critical to meet the increasing demand for high power and performance. Thermal interface materials (TIMs) play a key role in dissipating heat away from the microelectronic chip and hence are a crucial component in electronics cooling. Challenges persist with overcoming the interfacial boundary resistance and filler particle connectivity in TIMs to achieve thermal percolation while maintaining mechanical compliance. Gallium-based liquid metal (LM) capsules offer a unique set of thermal-mechanical characteristics that make them suitable candidates for high-performance TIM fillers. This dissertation research focuses on resolving the fundamental challenges posed by integration of LM fillers in polymer matrix. First, the rupture mechanics of LM capsules under pressure is identified as a key factor that dictates the thermal connectivity between LM-based fillers. This mechanism of oxide "popping" in LM particle beds independent of the matrix material provides insights in overcoming the particle-particle connectivity challenges. Second, the physical barrier introduced due to the polymer matrix needs to be overcome to achieve thermal percolation. Matrix fluid viscosity impacts thermal transport, with high viscosity uncured matrix inhibiting the thermal bridging of fillers. In addition, incorporation of solid metal co-fillers that react with LM fillers is adopted to facilitate popping of LM oxide in uncured polymer to overcome this matrix barrier. Solid silver metal additives are used to rupture the LM oxide, form inter-metallic alloy (IMC), and act as thermal anchors within the matrix. This results in the formation of numerous thermal percolation paths and hence enhances heat transport within the composite. Further, preserving this microstructure of

interconnected multiphase filler system with thermally conductive percolation pathways in a cured polymer matrix is critical to designing high-performing TIM pads. Viscosity of the precursor polymer solution prior to curing plays a major role in the resulting thermal conductivity. A multipronged strategy is developed that synergistically combines reactive solid and liquid fillers, a polymer matrix with low pre-cure viscosity, and mechanical compression during thermal curing. The results of this dissertation aim to provide fundamental insights into the integration of LMs in polymer composites and give design knobs to develop high thermally conducting soft composites.

DEDICATION

This dissertation is dedicated to my parents, who taught me always to dream big and work hard to make them a reality. To my sister, who always stood by my side and believed in me.

ACKNOWLEDGMENTS

Firstly, I would like to express my gratitude to Dr. Konrad Rykaczewski and Dr. Robert Wang for being my Ph.D. advisors and for all their support throughout my Ph.D. journey. I would like to thank you for your guidance, patience, and encouragement that has helped me in my research. Your mentorship is a source of inspiration, and I am grateful for your insightful discussions and scientific advice. Thank you for your contributions and sharing your wisdom in this field of research that has helped me grow my skill sets for the rest of my research career. Your dedication, intellectual virtues, scientific perspective, timely advice, and motivation are rare to find, and you are mainly responsible for the kind of professional working person I am today.

I would also like to thank my committee members, Dr. Beomjin Kwon, Dr. Gaurang Choksi, and Dr. Patrick Phelan, for serving on my committee. Additionally, I thank Dr. Matthew Green and his graduate student Jae Sang Lee for extending their help and expertise. I also extend thanks to all my lab mates for their support and always being ready to extend their help: Dr. Matt Ralphs, Dr. Wilson Kong, Ashish Rana, Najam Shah, Shreyas Kanetkar, Dr. Zhongyong Wang, Dr. Praveen Kotagama and Dr. Prathamesh Vartak.

I am highly grateful to Intel Corporation for funding my Ph.D. and being an amazing employer. I cannot thank my Intel work family enough for supporting, encouraging, and believing in me: Dr. Gaurang Choksi for always being there as a professional and personal life mentor, Dr. Ravi Mahajan, Dr. Weihua Tang, Dr. Je-Young

Chang, Dr. Edvin Cetegen, Dr. Pramod Malatkar, Divya Mani, Sushrutha Gujjula-Thank you all for your unwavering support. I am so grateful to have a work family that is thinking about my well-being and career and for seeing the potential in me.

I would like to give special thanks to my parents for everything they have done and continue to do for me. Thank you for educating me with the moral values that guide all my decisions and for your unconditional support. I thank my sister for her continued support and for being there through all the ups and downs of my research. I also thank all my friends for providing the support and friendship I needed. Special mention to Aditya Dabak, Anuja Papriwal, and Ravishankar Kammula for being there with me and supporting me throughout this journey.

TABLE OF CONTENTS

Page

LIST OF TABLES

Table Page

LIST OF FIGURES

Figure Page

Figure Page

Figure Page

Figure Page

Figure Page

CHAPTER 1

1. INTRODUCTION

1.1 Thermal Interface Materials for Electronics Cooling

1.1.1 Motivation

Efficient thermal management plays a critical role in the development of high-performance electronics, soft robotics, and flexible electronics to ensure that the devices function reliably. Advancements in the semiconductor industry have enabled the packaging of microelectronic chips with increased transistor densities into complex architectures that help to support high computational power without compromising the compactness of devices. However, this causes highly localized heat generation, resulting in undesirable thermal hot spot regions that limit computer processor performance.[1–5] Heat dissipation strategies are required at the package and system level to meet this increasing cooling demand for microprocessors. Thermal interface materials (TIMs) are critical enablers in developing an efficient thermal management system to support high-performance electronic devices.[6] TIMs can be a component of both package and system cooling. They play a critical role in removing heat away from the heat-generating components by reducing the thermal resistance path between the heat source and the cooling solution, as illustrated in Figure 1.1a and b.

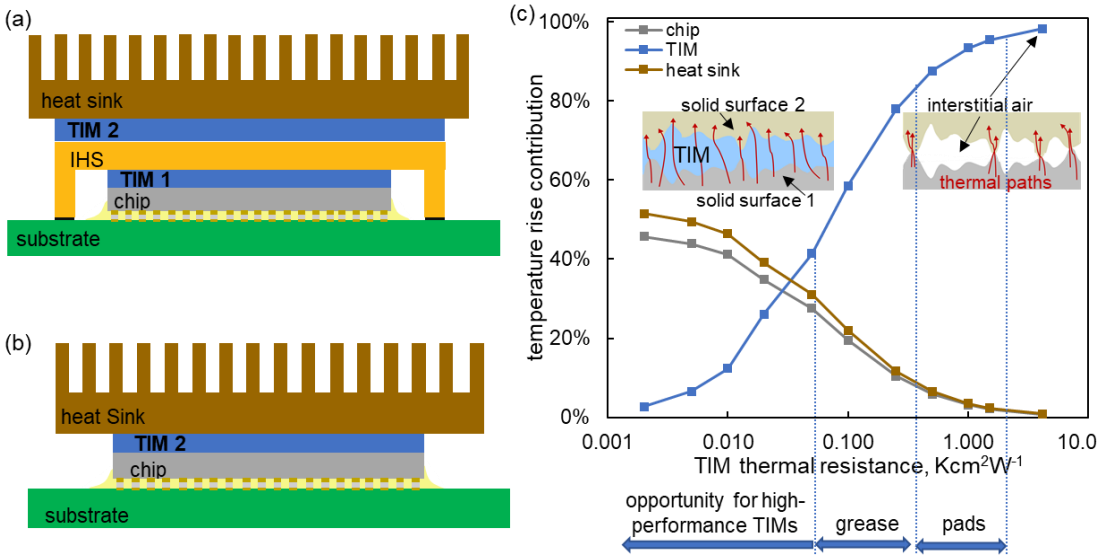

Figure 1.1: Schematic illustrating the use of TIM in a typical electronic package at (a) both package level between chip and integrated heat spreader (IHS) and system level between IHS and heat sink, and (b) only system level between the chip and heat sink, and (c) graph illustrating the temperature rise contribution by chip, heat sink and TIM for a range of thermal resistances representing the commonly used commercially available TIMs when a uniform power source is applied on the chip

The ideal cooling scenario is for the chip to be in perfect physical contact with the cooling solution, thus creating the least resistance path for heat transfer. However, given any two solid surfaces in contact, there is an interfacial gap created due to the microscopic roughness of the surfaces. These gaps substantially reduce the physical contact between the solid bodies and hence restrict the heat flow.[7] TIMs bridge these gaps and form thermal connections between surfaces by replacing the low conducting air gaps (0.024 W m^{-1} K^{-1}) with higher thermal conductivity material. Assuming that the micro roughness of the solid surfaces results in a 10 µm air gap, without any TIM material, the heat flow from the chip to the cooling solution will be restricted due to the low thermal conductivity of air which translates to a high thermal resistance ~4.2 K cm^{-2} W^{-1}. Additional factors like the warpage of the chip further reduce the contact area

between the chip and the heat spreader, resulting in increased thermal contact resistance.[8] Hence, TIMs need to have conformability to fill the surface irregularities, minimize stress on the components, and improve heat flow. Thermal grease, gap pads, gap fillers, and phase change materials are commonly used TIMs that offer moderate thermal conductivity (~1-7 W m^{-1} K^{-1}) and perform reliably under thermal cycling.[8–12] Considering the thermal stack-up of chip-TIM 2-heat sink Figure 1.1b, the contribution by each of these components is calculated assuming the chip and heat sink resistance to be 0.033 K cm^{-2} W^{-1} (0.5 mm thick silicon chip), and 0.038 K cm^{-2} W^{-1} (1.5 mm thick copper heat sink) respectively. The commonly used TIMs' contribution to the device's temperature rise can range from ~95% to ~40% (1.5 K cm^{-2} W^{-1} to 0.05 K cm^{-2} $W^{-1,}$ respectively), as shown in Figure 1.1c. Thus, the performance of TIMs can be a major bottleneck in supporting the high-power requirements of advanced electronics. The development of high-performance TIMs can help reduce their contribution to the overall temperature rise to less than 25%; hence, advancements in TIM technology is one of the key enablers in addressing thermal management challenges in future-generation electronics.

Most commonly used TIMs in electronics cooling are polymer-based composites consisting of a polymer matrix with filler particles. The matrix renders the composites' desired mechanical and adhesive characteristics and ensures compatibility with the mating surfaces.[13,14] The fundamental gaps and challenges that need to be addressed for the development of low thermal resistance polymer-based composites will be discussed in the following sections.

1.1.2 Polymer Composites as TIMs

Polymer composites offer unique functional properties for various applications like sensors, energy storage, conducting electrodes, electronics cooling, and biomedical applications.[13,15–18] Polymer-based TIMs offer the benefits of mechanical compliance, ease of fabrication, corrosion resistance[19], etc., due to the presence of base matrix material that helps to reduce the contact resistance between the mating surfaces. However, the inherently low thermal conductivity of this base polymer matrix (e.g., 0.2−0.3 W m^{-1} K^{-1})[20] becomes a bottleneck in the thermal transport within the composites. High thermally conducting rigid filler materials such as alumina, graphene, copper, etc., are included in the polymer matrix to enhance the thermal conductivity of the composites.[21–26] Increasing the volume fraction of these rigid particles enhances thermal properties, but has detrimental effects on other properties like viscosity, mechanical modulus hence rigidity, strength, etc.[27–30]

In order to design a TIM with high thermal conductivity, it is important to know the various factors impacting the effective thermal resistance. The intrinsic thermal conductivity only accounts for the intrinsic resistance of the TIM material (R_{TIM}). Contact resistance (R_c) between the TIM and the mating surfaces arising from the roughness of surfaces in contact must be accounted for to get the effective thermal conductivity (k_{eff}). [31] With the inclusion of particles in a base polymer matrix, the interactions between the particles themselves and between particles and matrix also play a critical role in the

composite thermal properties and contribute to thermal boundary resistance (R_b).[32] Thus, the total thermal resistance (R_{th}) and the effective thermal conductivity (k_{eff}) is given by

$$R_{th} = R_{TIM} + 2R_c$$

$$k_{eff} = \frac{thickness}{R_{th}}$$

Any change in the material properties within the composite contributes to the boundary resistance. Interfacial contact thermal resistance between the fillers and scattering of phonons due to the thermal mismatch of high thermal conductivity solid fillers and low conductivity matrix within the TIM increases the thermal resistance and hence restricts the thermal conductivity of the composite.[33] Figure 1.2 illustrates the different thermal resistances that govern the thermal transport in polymer TIMs.

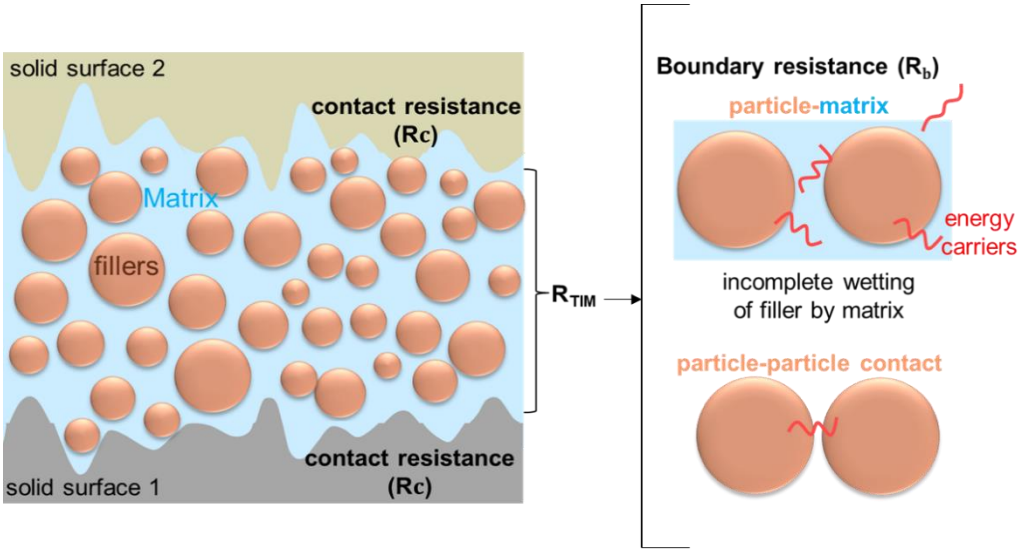

Figure 1.2: Thermal resistances in a typical polymer TIM

Each thermal resistance contributor in the composite TIM can be treated as a design knob and hence can be used to cleverly design and tune the composites. Starting with the selection of the filler, conventionally-used rigid filler particles have a poor

physical contact due to the point contact between adjacent fillers, and inherent interfacial resistance between the particles limits the effective thermal conductivity of the composites. Methods like microwave welding[34] have been used to increase the thermal conductivity in composites by increasing the particle contact area and hence overcoming the filler limited point-point contact area.

With the inferior thermal conductivity of matrix material, it becomes important to ensure thermal connectivity between fillers and polymer matrix is established in the composites. Formation of the thermal percolation network and strategies to enhance thermal transport are also dependent upon the matrix properties. Considering the most commonly used polymer TIMs, the matrix can be uncured (grease) and cross-linked (pads).[8–12] Each has merits and shortcomings in its overall thermal-mechanical performance. Thermal greases have lower thermal resistance because of the ability to achieve thin bond line thickness. The low viscosity of the matrix allows it to flow easily to fill the surface irregulates, hence offering the opportunity to reduce contact resistance. However, they have pump-out issues during thermal cycling due to the coefficient of thermal expansion (CTE) mismatch between the packaging components as shown in Figure 1.3a and are susceptible to phase separation[28–30] as shown in Figure 1.3b.

With the cross-linking of the matrix, thermal pads overcome the issue of pump-out; still, the cured polymer introduces challenges with achieving high thermal performance due to limitations with the amount of filler that can be added[35] and the thickness of the pads. Commonly used silicone elastomers have low modulus that helps with better compressibility and overcoming the stresses due to large CTE mismatch in the

electronic packages during thermal cycling.[28,29] In order to improve the thermal properties of thermal gap pads, the volume fraction of filler loading is a commonly used parameter to form thermal percolation paths. While this enhances the intrinsic thermal conductivity of the gap pad, the mechanical design of the composite suffers from an increase in rigidity.[18,36] as shown in Figure 1.3c. With the reduced conformability, contact resistance increases and hence the overall effective thermal conductivity of the pad reduces. The introduction of non-rigid filler particles can help achieve a thermal-mechanical design balance in the development of thermal pads.

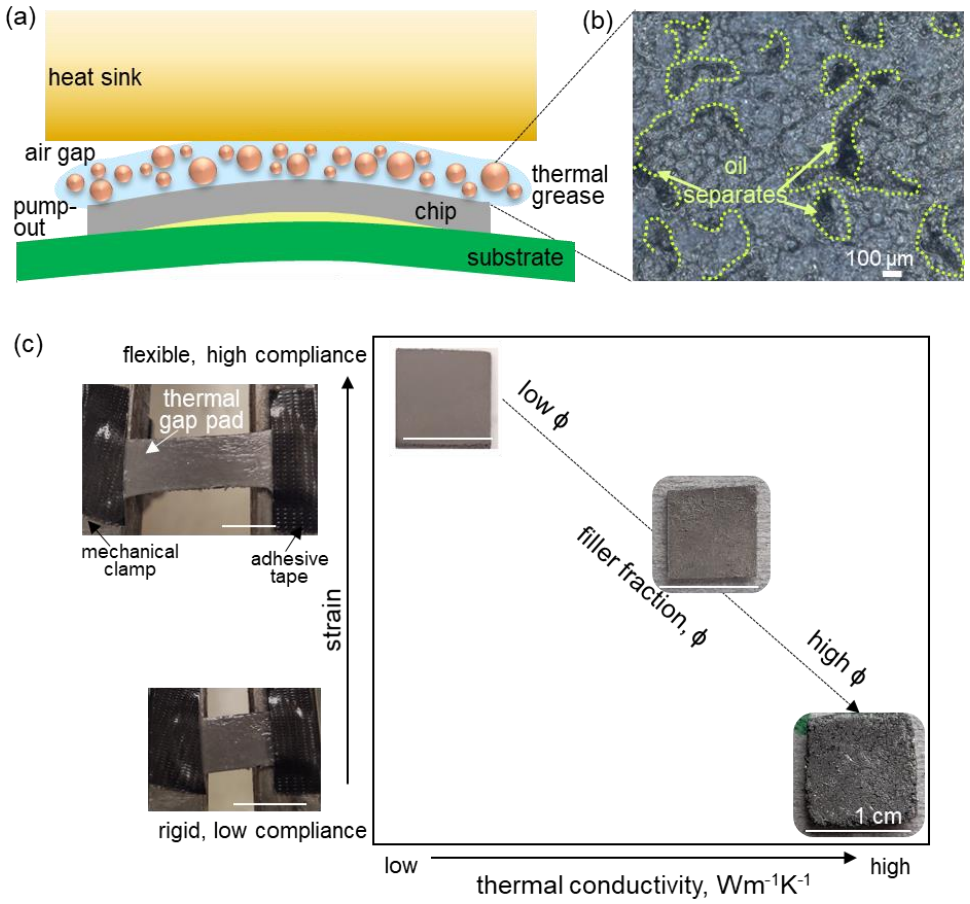

Figure 1.3: (a) Schematic for the stresses induced in thermal grease with temperature changes due to CTE mismatch, (b) Microscale morphology of grease highlighting oil matrix separating from fillers, and (c) Impact of filler volume fraction on the mechanical and thermal properties of thermal gap pads

In addition to overcoming the thermal resistances within the polymer composite, effective thermal networking of fillers is required to enhance the thermal percolation. The formation of thermal conduction pathways in the integrated filler-matrix system is required for achieving a high thermal conductivity TIM composite. Methods like filler alignment and out-of-plane orientation using magnetic field[37–39], mechanical cutting[40], electrical field[41,42], as well as sample straining,[43,44] hot pressing,[45] press-rolling,[14] and chemical vapor deposition[46] have been used to form the percolation network.[18] Integration of the strategies to reduce filler, matrix interfacial thermal resistance and improving thermal conduction pathway can help develop TIMs with enhanced functional properties.

1.2 Improving Filler-Filler Connectivity and Filler-Matrix Thermal Bridging

1.2.1 Liquid Metals as Fillers

Gallium-based room-temperature LMs (*e.g.*, elemental Ga, eutectic GaIn, and eutectic GaInSn) have recently emerged as a unique filler material for composites in flexible electronics, soft robotics, and TIMs.[36,47–51] These LM materials simultaneously provide a unique combination of metallic properties (*i.e.*, thermal and electrical conductivity) with the conformability of a liquid. This allows for high-volume fraction microdroplet incorporation into polymer composites without degradation of the mechanical properties.[36,50,52] Recent works have explored LMs in soft polymers, focusing mainly on the electrical properties with LM being used as electrical anchors between

conductive fillers.[14,49] However, the electrical transport properties are not transferable to thermal transport properties.

These room-temperature LMs, such as eutectic GaIn or GaInSn have a thermal conductivity of 20-30 W $m^{-1} K^{-1}$. However, these liquid metals are not widely used because they are relatively difficult to apply (high surface tension), can pump out during thermal cycling, and degrade other metals in the package (highly reactive with other metals and causes corrosion, embrittlement etc.).[33,53] Recent research has suggested that these issues can be partially or fully mitigated by dispersing LM droplets within a grease [54–56] or cured polymer matrix.[26,36,52,57,58] as shown in Figure 1.4. However, the inclusion of LM droplets alone leads to limited improvements in polymer composite thermal conductivity (e.g., for an extreme volume fraction of 80% LM-fillers, an effective composite thermal conductivity of 5.3 W $m^{-1} K^{-1}$ in oil,[59] 9.9 W $m^{-1} K^{-1}$ by including hybrid liquid metal-coated silicon carbide particles in silicone oil,[56] 6.7 $Wm^{-1}K^{-1}$ in elastomer which increases to 11 W $m^{-1}K^{-1}$ upon stretching,[36] 10 W $m^{-1} K^{-1}$ in polydimethylsiloxane (PDMS) matrix by a mechanical mixing fabrication technique [26]., ~1.7 W $m^{-1} K^{-1}$ by vacuum-assisted infiltration,[35] 4 W $m^{-1} K^{-1}$ by magnetic alignment,[38] and 4.8 W $m^{-1} K^{-1}$ by adopting sacrificial templating[60]). There are limited explorations in designing and characterizing LM-based soft composites to improve thermal performance. This dissertation work will address this gap by first outlining the thermal resistances in a LM composite system in the next section.

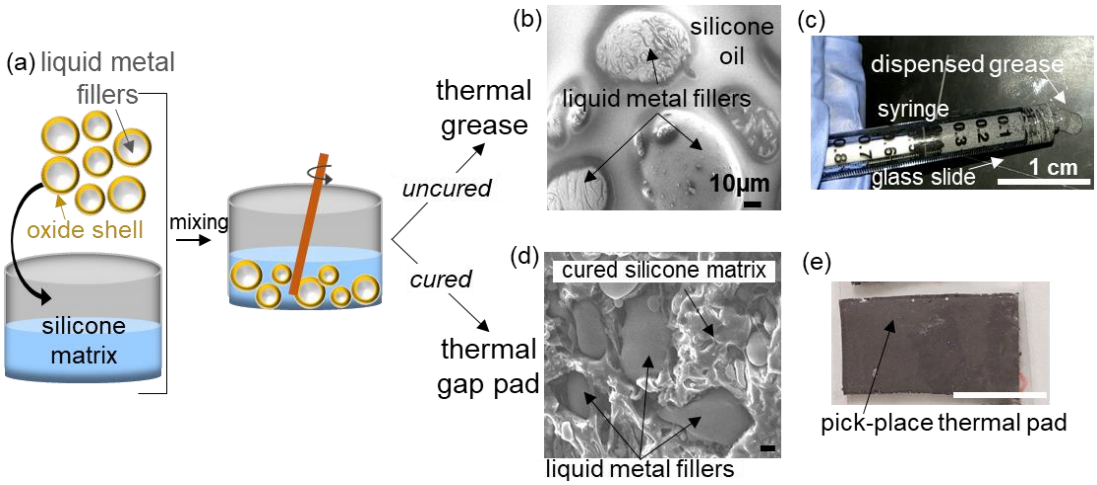

Figure 1.4: LM based composites explored for thermal characterization: (a) Schematic illustrating the incorporation of LM in polymer matrix, (b) electron micrograph showing LM droplets encapsulated in uncured silicone oil matrix resulting in formation of thermal grease with 50 vol% LM filler, (c) dispensing LM-based grease using syringe, (d) electron micrograph showing LM droplets embedded in cured silicone matrix resulting in formation of thermal gap pad with 50 vol% LM filler, and (e) LM-based gap pad for easy pick and place applications

1.2.2 Thermal Resistances in the LM Composite System

The LM fillers are actually LM capsules that are surrounded by a native oxide shell that is 0.5−2.5 nm thick.[52,61–67] This oxide shell provides a self-healing and mechanically flexible membrane that contains liquid metal. The oxide skin mainly consists of β-gallium oxide (Ga_2O_3) which rapidly forms around the LM in ambient conditions.[68] Even though only a few nanometers thick, this layer is mechanically robust, imparts viscoelastic behavior to LMs by behaving like a solid layer around the liquid metal and adds yield stress to the LM fluidic core. These characteristics of the oxide layer stabilize LMs and allow them to form stabilized complex structures.[61–66,69,70] However, the oxide layer serves as a barrier in the heat transfer path and impairs thermal transport for two reasons. First, the amorphous oxide has a thermal conductivity much lower than

that of LM.[33] Second, the oxide shell can wrinkle on multiple length scales and this wrinkling significantly impairs heat transfer between adjacent capsules.[63,71] The wrinkled microcapsule surfaces are evident in Figure 1.5b-d. These two thermal resistances are unique to the polymer composites with LM filler as illustrated in Figure 1.5. In addition to these LM filler resistances, the other thermal resistances like contact resistance and LM filler to matrix thermal resistance also exist similar to a typical polymer-based composite shown in Figure 1.2 and discussed previously.

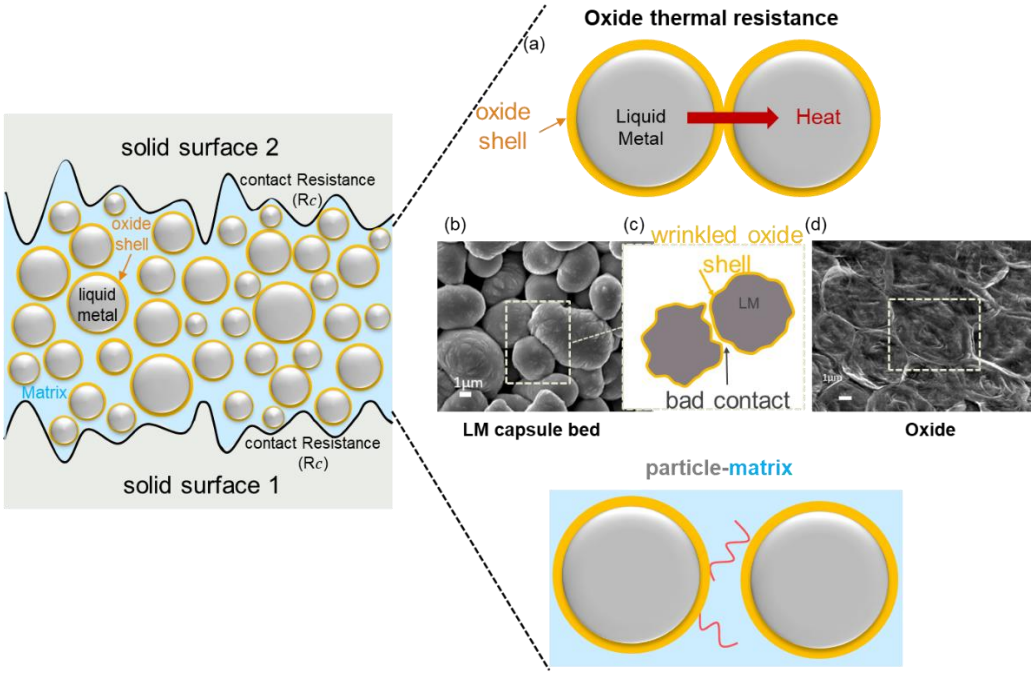

Figure 1.5: Thermal resistances in a LM-based polymer composite: (a)-LM oxide layer on the LM fillers serve as a barrier to the heat flow, (b) LM capsule beds with wrinkled oxide layer, (c) schematic illustrating how the wrinkles on oxide layer result in a bad contact causing the thermal resistance to increase, and (d) electron micrograph showing the oxide shells when liquid metal is drained out.

Regarding the role of R_c, since LM possesses the fluidic attributes of low viscosity and liquid-like flowability, R_c between LM and the mating surfaces arising from

roughness of surfaces in contact must be significantly low compared to the commonly used thermal greases with commonly used solid fillers in them. The R_{TIM} and R_c of pure gallium are estimated based on the thermal resistance measurements conducted with an in-house built stepped-bar apparatus (SBA) following the ASTM D5470 standard.[26,72–75] To decouple the contact resistance between the samples and the measurement system, the thermal resistance is measured as a function of sample thickness. A linear trend is fit such that it separates the R_c (y-intercept of the linear trendline) from the R_{TIM} (inverse of slope) as shown in Figure 1.6. The intrinsic thermal conductivity of 37.0 W m^{-1} K^{-1} for pure gallium is obtained and the contact resistance is 0.016 K cm^2 W^{-1}. As shown in Table 1.1, the R_c for a commercial thermal joint compound (Wakefield Type 120 silicone) is ~15 times higher than gallium LM. Thus, LM offers superior conformability and hence lower contact resistance compared to conventional thermal greases.

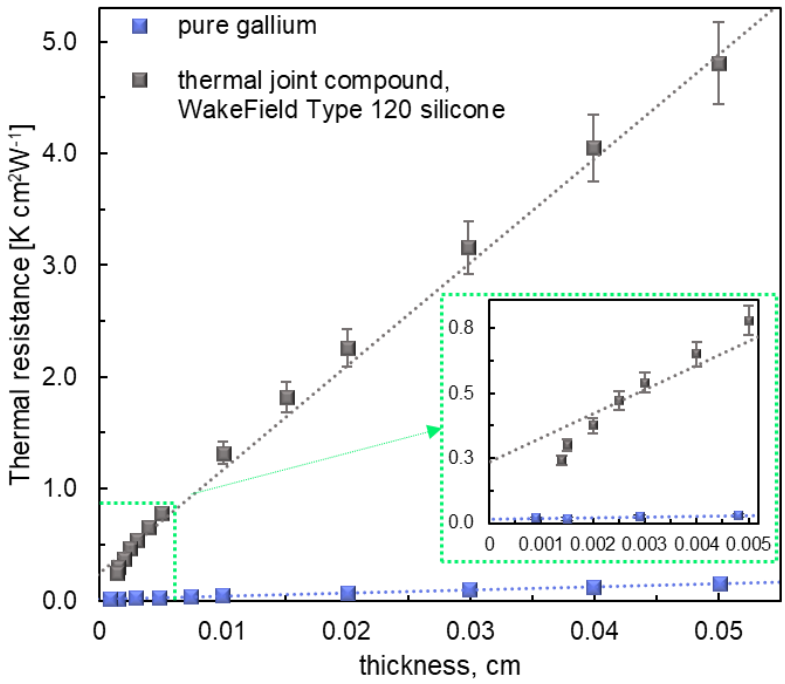

Figure 1.6: Thermal resistance versus thickness for pure gallium and commercially available thermal joint compound (Wakefield Type 120 silicone)

Table 1.1: Intrinsic thermal conductivity and contact resistance for LM and thermal joint compound

	Thermal joint compound (Wakefield Type 120 silicone)	Pure gallium
contact resistance (R_c)	0.24 K cm ^{2} W^{-1}	0.016 K cm^2 W^{-1}
thermal conductivity	1.1 W m^{-1} K^{-1}	37.0 W m^{-1} K^{-1}

1.2.3 Deformation Characteristics of LM Composite System

Ideally, the TIM should remain elastic throughout the compression cycle, and the TIMs should have low stiffness and high recovery behavior, which will help minimize the contact resistance. If the strain recovery is high, it could cause delamination and harm the thermal performance.[28,29] For polymer TIMs to be efficient and reliable, the mechanical properties that mainly govern the thermal performance are modulus, CTE, compression setting, adhesion, and strength.[28]

Tensile, compression, and shear tests are often used for modulus measurements of polymer TIMs. A polymer with low filler content will show a low storage modulus in tensile testing (dynamic strain applied over a range of temperature[76]), indicating the softness of the composite. Compression tests help to understand the strain behavior as well as recovery characteristic of TIMs that can be used to compare the permanent deformation of composite pads. Higher is the permanent deformation in compression during temperature cycling, the TIM has a larger extent of delamination in tension. Shear strain testing helps determine TIM's failure modes under reliability conditions. For example, whether the polymer TIM is undergoing temperature cycles (dynamic warpage-

based deformation like pump-out) or maintained at a constant temperature, an increase in the storage modulus of the TIM in the latter case indicates a hardening of the material, which can lead to delamination and hence thermal performance degradation during reliability. It is also important to determine the recovery characteristics of the TIM to its original shape upon deformation. Lower compression set values indicate better shape recovery, which will better fill voids after the TIM is compressed and allowed to recover. Other tests like adhesion and CTE measurements have been explored to characterize the mechanical characteristics of TIMs used in microelectronic packages.[28]

With the inclusion of solid fillers in the polymer composite, it is important to maintain a low elastic modulus to fill voids between the mating surfaces. The composite pad should have a low shear modulus so that it can conform and improve adhesion. Stiffer or rigid TIMs have a high modulus that prevents them from conforming to mismatched surfaces. This makes them less efficient in conducting heat due to the microscopic gaps not being filled by the stiffer TIMs. Decreasing the hardness could lead to increased creep behavior under deflection and decreased strain recovery on removing the compressive stress.[29]

Using LM fillers can lead to unique advantages to achieve the desired mechanical properties. The storage modulus in cured PDMS increases with the increase in vol% of liquid metal Galinstan. This means the introduction of LM as fillers increases the composite's stiffness compared to the PDMS without any fillers and hence will be less complaint than only PDMS composite. However, the impact of increase in the storage modulus with solid fillers is found to be larger than with liquid metal fillers.[77] The benefit

of including LM as fillers is evident from the better compliance characteristics of the composites. Recent works have shown that higher filler loading to improve thermal properties can be achieved with the LM fillers in polymer composites while maintaining compliance and being relatively soft compared to the solid-filled composites. In some of the multiphase filler systems explored for soft composites, it was found that the mechanical response degraded faster than the increase in thermal conductivity.[36]

The silicone composites with LM droplets as inclusions are stiffer than pure silicone. Young's modulus of the silicone composites with EGaIn increases with the increase in the volume fraction of the LM fillers[66]. It is reported that on increasing the filler loading of EGaIn in silicone composite from 0% to 50%, the elastic modulus increased from 85 kPa to 235 kPa.[66]

Eshelby's theory of composites has been used to get the composite modulus E_c that has LM droplets with effective Young's modulus E_{eff} embedded in elastomer with modulus E_s.[66,78] Previous works have used this theory to predict the modulus of composites with LM fillers using this model. For silicone-based elastomer composites with EGaIn as liquid metal fillers (0 to 50 vol%), Bartlett et al.[66] used E_{eff} for EGaIn as 320 kPa which treats the LM particles as soft inclusions rather than liquid inclusions. This was attributed largely to the oxide shell of LM droplets that provide stiffness to liquid metals and to the lack of particle interaction between the liquid metal fillers at volume fractions upto 50%.[66] Koh et al.[77] used the modulus of galinstan E_{eff} as 80 kPa to match their data with Eshelby's model at 30 and 50 vol%. Using the same value for 70 vol% led to underestimation of the modulus which was attributed to the increase in

presence of oxide as particle size decreases, inhomogeneity in particle size and increased interaction between particles.[77]

The stiffness of composites with liquid inclusions is controlled by two length scales: First is the elastocapillary length L_e = surface tension γ /Elastomer Young's modulus E_s, when surface tension plays a significant role. This factor contributes to the stiffening of the composite only if the liquid inclusions in the elastomer are small relative to this length.[78] The second is the length corresponding to the liquid droplets with thin, stiff interfaces. If the liquid inclusions are smaller than $L_i=E_ih/E_s$ (where h=thickness of interfacial layers, E_i=Modulus of interfacial layer), then the interfacial layer is important, and the presence of droplets will stiffen the composite. Eshelby's theory can be used to demonstrate the effect of these two interfacial phenomena for the droplets embedded in solids.[78]

Recently Style et al. described an approach to use the dilute Eshelby's model to predict that LM droplets of radius 10μm will stiffen the elastomers with modulus less than 6 MPa.[78] This assumes that there are two entirely uniform phases in the composite and the oxide shell for the LM droplet is a stiff interfacial layer and the modulus of the droplet is found to be $E_{eff} \approx E_ih/R$ (where E_i= gallium oxide modulus, h= thickness of the oxide shell, R = radius of the LM droplet). Using these assumptions with the equation[79–81] below gives the droplet size that can increase the composite stiffness.

$$E_c = E_s \frac{1+\frac{2E_{eff}}{3E_S}}{\left(\frac{2}{3}-\frac{5\phi}{3}\right)\frac{E_{eff}}{E_S}+\left(1+\frac{5\phi}{3}\right)}$$

For liquid inclusions E_{eff} = 0 (no surface tension) and for rigid particles, E_{eff} = ∞. The inclusion of LM droplets can result in a composite with stiffness anywhere between the liquid and rigid limits.[78] For liquid metal droplets, stiffening of composite occurs when the radius of the droplets is less than length Li=Eih/Es.

The mechanical and thermal properties of composites are a function of the type of filler particles, compositional tuning, and type of polymer matrix. These functional properties can be tuned to evaluate the design trade-offs required to achieve high thermal performance polymer pads with compliance and can be customized to the requirements of different applications, specifically TIMs. The identified mechanisms to tune the functional properties can further be extended to other applications of LM-composites like electronic inks, stretchable electronics, wearable sensors, soft robotics, etc.

1.3 Thermally Enhanced Liquid Metal Composites with Tunable Thermal-Mechanical Properties

1.3.1 Fundamental Gaps and Challenges

The LM-based polymer composites developed so far show a moderate thermal conductivity value even upon increasing the filler volume fraction. Other techniques such as elongation and mixing solid conductive particles also only show a moderate increase in the thermal performance of these composites. The ideal scenario for thermal transport in the polymer system will be to have multiple thermal percolation pathways via connecting the LM fillers within the polymer matrix as shown in Figure 1.7. However, to realize this goal, some fundamental gaps need to be addressed, like the LM filler-filler

interface resistance, bridging the LM fillers in the polymer composite, and preserving the thermal connectivity within the polymer matrix.

In this dissertation work, I put forward the underlying mechanisms that govern the functional properties, specifically thermal and mechanical of LM composites. Specifically, my work addresses ways to overcome the thermal resistance paths in the composite system and identifies the control knobs to tune the functional characteristics of LM-based composites.

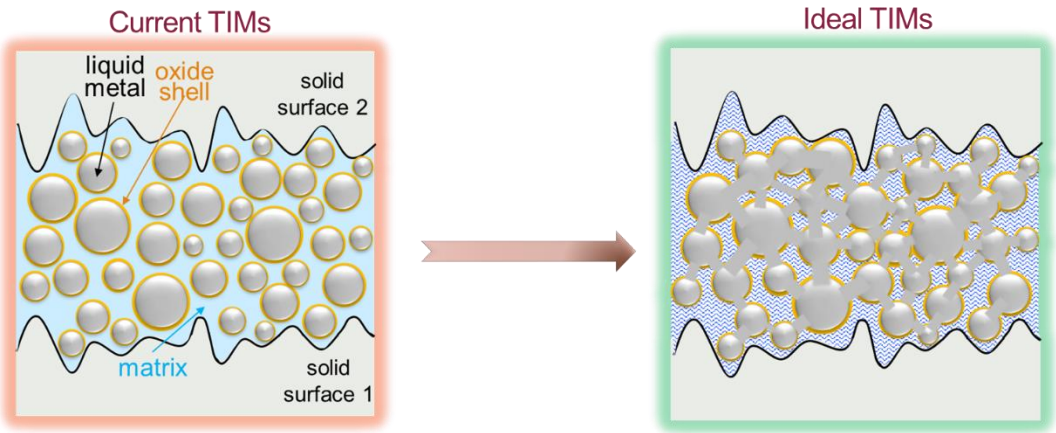

Figure 1.7: Concept of an ideal LM based polymer TIM

1.3.2 Assertions

LM as thermal fillers can be utilized to their full potential by rupturing their oxide shells. Once the oxide shells "pop," the particles can directly bridge and establish filler-to-filler contact. With the oxide shell ruptured, an area-contact will be established rather than a point contact formed if rigid particles are used. Thus, the impact of "popping" the oxide shell will be three-fold: eliminating the additional thermal resistance contributed by the low thermally conducting oxide shell, reducing filler boundary resistance by

establishing area contact between the particles, and establishing multiple conductive pathways for heat flow.

For the thermal composite to have high thermal conductivity, effective bridging of fillers needs to be induced in the polymer matrix to form an interconnected particle network. Thermal percolation of LM microdroplets requires two physical barriers to be overcome. First, the LM droplets must directly contact each other through the polymer matrix. For this to happen, the matrix needs to be displaced effectively from in-between the LM droplets for them to connect and form heat conduction pathways. Properties of the matrix like viscosity, and filler processing can be tuned to obtain bridging on LM fillers in the polymer matrix. Second, the native oxide shells now need to be ruptured effectively. The addition of solid metal reactive co-fillers and application of pressure will further help to achieve “popping” of the oxide shell in the matrix by forming inter-metallic alloys and will act as additional paths that aid in connecting LM fillers. The synergy between thermal transport and mechanical compliance can be achieved by tuning the hybrid fillers ratio, filler processing technique, and matrix viscosity.

Preserving the bridging of the LM fillers in cured polymer composites will require fabrication techniques that involve external stimuli like pressure, temperature to activate the thermal connectivity in the matrix post-curing. The thermal and mechanical properties of the resultant composite pad will be impacted by the filler size, filler processing, ratio, type of hybrid filler, and the activation mechanisms used. Designing a customized fabrication process will also help in reducing the contact resistance of the polymer composites.

1.3.3 Dissertation Scope and Outline

This dissertation work explores the underlying fundamental mechanisms that govern the functional properties (*i.e.,* thermal and mechanical properties) of soft polymer composites. My research findings can be used to design LM-based polymer composites with enhanced functional properties that can be tuned depending on the applications. The key fundamentals investigated in this work will serve as guidelines for tuning polymer composites' thermal and mechanical characteristics. Figure 1.8 shows the main framework of my research that I have developed to explore some of the fundamental concepts required for designing LM-based polymer composites. In this dissertation work, I pursue three research cores: 1) interfacial interaction of LM fillers, 2) polymer-rheology-dependent thermal network, and 3) external-stimuli-activated thermal pathways. These core areas are explored throughout my research work, with this chapter *i.e.,* Chapter 1 introducing the importance of development of thermally enhanced TIMs for electronic cooling, how the different thermal resistances in a polymer composite hinder the heat transfer and the introduction of LM as fillers. This chapter lays the foundation of the fundamental questions that will be addressed in the subsequent chapters.

Chapter 2 discusses the interfacial thermal resistances in LM fillers and ways to overcome the LM oxide skin thermal barrier. Here, I introduce a novel method for studying the rupture mechanics of beds composed of LM capsules in an air matrix. This isolates the effects of the oxide shell from the surrounding polymer. Through this simplified system consisting of LM capsule beds in an air matrix, I quantify the dependence of LM capsule rupture pressure on LM capsule age, size distribution and

oxide shell chemical treatment. This investigation reveals the importance of using freshly prepared LM capsules to get high thermal conductivity. I highlight how the oxide shell growth with time degrades the thermal properties of the LM capsules and hence use of aged capsules will adversely affect the thermal characteristics of the composite with LM fillers. Additionally, the size of fillers dictates the oxide rupture pressure and thermal conductivity. This work reveals that larger diameter LM capsules have higher thermal conductivity and can be ruptured more easily with less pressure. Further, the chemical treatment of the LM capsules facilitates oxide rupture and increases the thermal conductivity. This addresses the fundamental knowledge gap of how the oxide shells influence thermal transport in LMs. These new insights serve as guidelines for preparing optimal LM or hybrid LM-solid additives for soft polymer composites. This work is discussed in detail in Chapter 2.

Chapter 3 discusses the role of polymer viscosity in forming a thermal network between the LM fillers. With the incorporation of LM particles in a polymer matrix before cure, the matrix acts as an additional physical barrier. This work shows that tuning the viscosity of the uncured polymer helps to ease the bridging of LM particles. Reducing the oil viscosity helps displace the uncured polymer from in-between the fillers, facilitating direct filler contact during compression. This chapter reveals that tuning the matrix viscosity is not sufficient to achieve ample bridging of LM particles. I highlight the need to add reactive solid conductive fillers in conjunction with pressure and viscosity tuning to induce the oxide shell "popping" required to achieve thermal percolation. This work shows that the reactive solid metal fillers facilitate the popping of

LM oxide and act as thermal anchors that connect the LM fillers within the matrix via alloy formation. I highlight the importance of fabrication method in tuning the thermo-mechanical characteristics of the composites. Investigation of filler processing by sequential mixing and pre-mixing of LM-solid reactive fillers results in thermally enhanced composites with undesirable mechanical characteristics. This provides an understanding of the design knobs for controlling polymer composites' mechanical and thermal characteristics like matrix viscosity, filler composition, filler fabrication, pressure for thermal percolation, and mechanical compliance. The insights from this chapter will serve as a key to developing future highly conducting LM-based thermal pads. The knobs identified can further be extended in developing polymer composites with tunable properties for other applications like sensors, wearables, and electrical interconnects. Chapter 3 covers the details of this work.

Chapter 4 discusses the importance of using a polymer matrix with tuned pre-cure viscosity and using compression during composite curing as an external stimulus to activate thermal pathways. This chapter reveals that employing compression as an activation strategy during the fabrication of the composites helps to preserve the thermal percolation pathways and reduces the interfacial resistances. I discuss the strategy that synergistically combines the reactive solid and liquid fillers, polymer matrix with low pre-cure viscosity and mechanical compression during thermal curing. I highlight the need for a low viscosity matrix material that can be cured to develop an easy-to-use, pick-and-place thermal pad with enhanced thermal properties.

Chapter 5 summarizes my dissertation work and I present the overall conclusions and discuss potential future research directions. I discuss some on-going explorations with processing and activation techniques, filler compositional tuning and size effects using hybrid fillers.

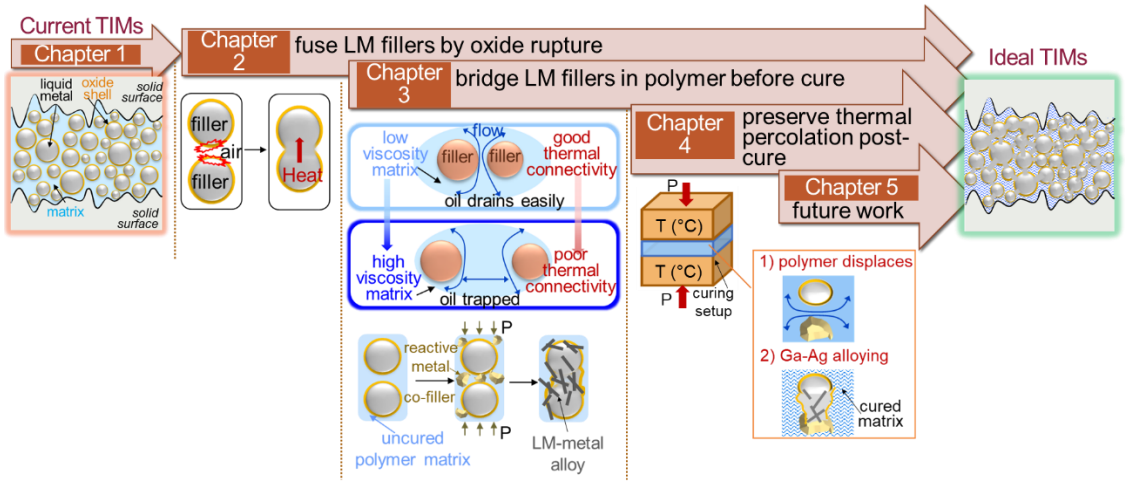

Figure 1.8: Research framework developed to explore fundamentals for designing LM-based polymer composites

CHAPTER 2

2. THERMAL TRANSPORT VIA LIQUID METAL OXIDE SHELL RUPTURE

2.1 Introduction

This chapter discusses the LM oxide rupture mechanism with a focus on the thermal transport in LM capsules. As explained in the earlier sections, the thin native oxide degrades the heat transfer between the LM capsules. In this chapter, I show that once ruptured, the liquid metal is released from the oxide shells and effectively bridges the microcapsules. This bridging of LM capsules is critical for achieving high thermally conducting LM-based TIMs.

This process has been studied from an electrical perspective, but the results do not fully translate to thermal applications because electrical transport requires only one single percolation path. The details in the below sections describe the detailed characterization and quantification of the different parameters of the LM capsule that impact the rupture of the oxide shell.

2.2 Fabrication of LM Capsule Bed

In order to study the rupture mechanics of LM capsules from a thermal perspective, LM capsule beds in an air matrix (*i.e.*, absence of any polymer material) are drop-casted on the bottom bar of the SBA setup (see Appendix A, figure A1). This is done to isolate the effects of the surrounding matrix material. Throughout this work, I

have used pure gallium instead of its eutectic alloys to focus on the rupture of the gallium oxide shell, since the presence of small amounts of indium and tin oxides is also possible in common gallium eutectic alloys.[82] The different diameter LM capsules are fabricated through ultrasonication following a selective sedimentation process.[83–86] The ultrasonication time and sedimentation process are used as modulators to control the average diameter of the capsules. The longer the sonication time, the smaller is the size of the capsules. The size distribution of LM capsules is obtained through scanning electron microscope (SEM) images and image analysis and is shown in Figure 2.1. Using this approach, I fabricated capsules with four different average diameters (0.7±0.5 μm, 1.4±0.5 μm, 3.1±0.8 μm, and 6.6±1.6 μm).

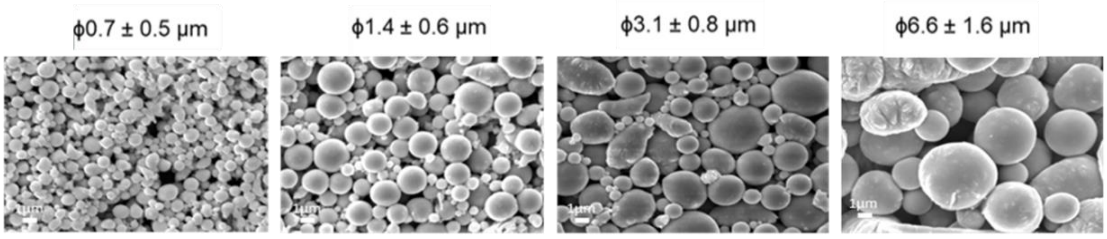

Figure 2.1: Representative SEM images of measured hydraulic diameters for capsule distributions with average diameters of (a) 0.7 ±0.5 μm, (b) 1.4 ± 0.6 μm, (c) 3.1 ± 0.8 μm, and (d) 6.6 ± 1.6 μm.[87]

2.3 Compression-Induced Oxide Rupturing Mechanism

Once the LM capsules are fabricated, I drop-casted them on the bottom bar of the SBA setup to form 1.5−2 mm thick beds of the LM capsules. Throughout the experiments, the bottom of the lower bar is maintained at a temperature of 30 °C, and the top of the upper bar is kept at 100 °C. These temperature settings resulted in a sample temperature above the gallium melting temperature. During the sample compression

experiments, I simultaneously measured the thermal (R_{th}) and electrical (R_e) resistances as a function of the thickness of the samples (t_{bed}), which is controlled through the applied compressive pressure in a stepwise manner.

2.3.1 Thermal and Electrical Characterization

The compression experiments are initiated when the upper bar touches the LM capsule bed. The changes in thermal resistance as a function of bed thickness, t_{bed} is measured and translated to the thermal conductivity using $k_{bed} = t_{bed}/R_{th}$. Figure 2.2 shows the changes in these values as a function of the normalized thickness of the capsule bed and pressure. The initial starting point of the compression experiments labeled as "I" is the extreme right of the plot and as the sample bed is compressed, with time, the bed thickness decreases and the plot proceeds to the left. This uncompressed state has a significant amount of air filling the interstitial space between the LM capsules resulting in poor contact between the particles. As the sample is compressed, the LM capsule bed transitions into different regimes that provide insights into the oxide rupture mechanics.

From fundamental and application perspectives, the most interesting information that can be inferred from the compression experiments is the compression level and pressure P_{peak} at which almost all LM capsules have been ruptured. This is shown as regimes "V" and "VI". Based on the data, the onset of these regimes occurs when the thermal conductivity peaks. The thermal conductivity peaks at a normalized thickness of around 0.25 in regime "V" where the majority of the oxide shells have ruptured. Further compression leads to physical leaking of the LM and oxide fragments. The thermal conductivity decreases during this part of the experiment because the leaking material is

predominantly LM. Consequently, the overall LM-to-oxide ratio changes as the sample is compressed. This is shown as regime “VI” which consists of large number of nearly completely drained oxide capsule shells.

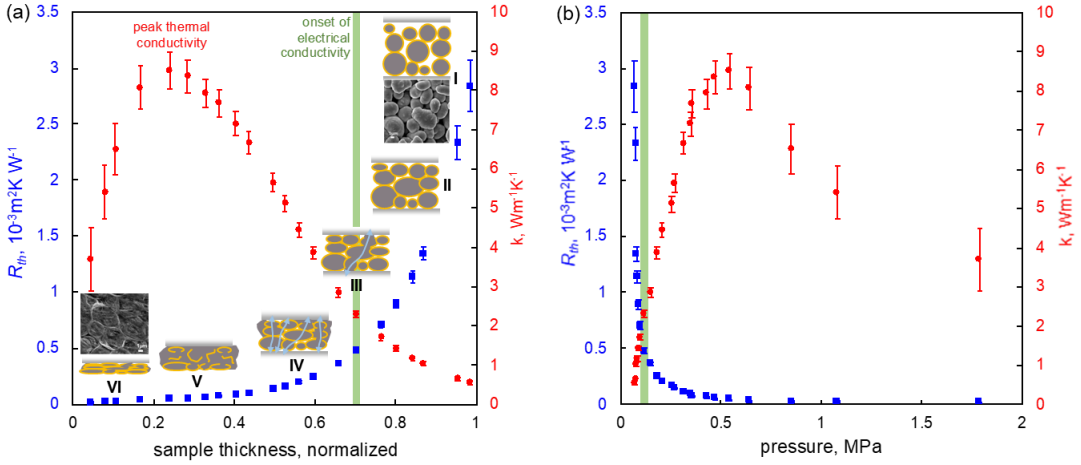

Figure 2.2: Typical plot showing the changes in thermal resistance (R_{th}) and thermal conductivity (k) during compression of a LM capsule bed as a function of (a) normalized sample thickness and (b) applied pressure. The schematic insets and SEM images in part (a) illustrate the microscopic processes underlying the observed trends in the macroscopic measurements. The liquid metal capsules in these experiments have an average diameter of 6.6 μm and a capsule age of 7 days.[87]

This investigation also highlights the difference in the electrical and thermal transport properties. In the “III” regime, where only a few capsules have ruptured, a sharp transition in the electrical conductivity at a normalized t_{bed} * of about 0.70 is observed as illustrated by the green vertical bar in Figure 2.2. However, the thermal conductivity of the bed at this compression level is less than half of its maximum value. This shows that the LM capsule bed is electrically conducting but still a poor thermal conductor. To significantly enhance the composites' thermal conductivity, many thermal conductive paths and consequently rupturing of a substantial fraction of capsules need to be established, as shown in Figure 2.3.

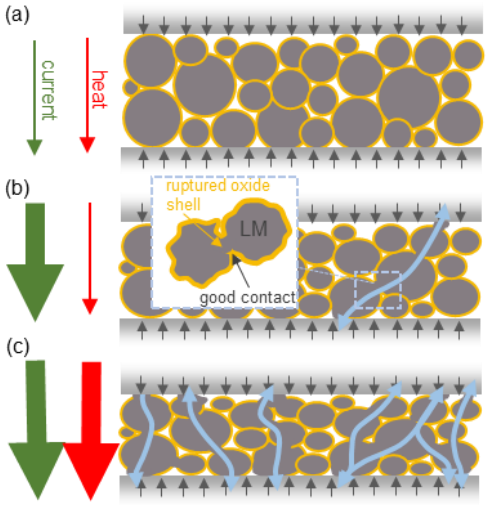

Figure 2.3: Schematics illustrating electrical current (green arrows) and heat flow (red arrows) in a bed of LM capsules: (a) Prior to compression, the LM capsule bed is electrically and thermally insulating (b) Mild compression of the bed leads to rupturing of a few large capsules and the formation of a percolation path (shown with blue arrow). This percolation path makes the capsule bed electrically conducting. (c) Substantial compression of the bed leads to rupturing of numerous capsules and formation of many percolation paths. Both electrical current and heat flow relatively easily in this state of the sample.[87]

2.4 Parameters Impacting Oxide Rupturing Process

The compression level or pressure, P_{peak}, at which the peak thermal conductivity, k_{peak} occurs is used as a metric to compare how various capsule characteristics impact the rupture dynamics of a capsule bed. Next, I use this methodology to quantify the impact of average capsule diameter and age on the rupture process of the LM capsule beds.

2.4.1 Capsule Age

The impact of oxide shell thickness on the pressure required to rupture it is conducted using LM capsules with an average diameter of 6.6 ± 1.6 μm. After fabricating the LM capsules, I stored them in ethanol and intermittently measured their properties over 25 days (*i.e.*, on days 1, 7, 12, and 25).

The peak thermal conductivity of 7-day-old samples was 28% lower than that of the freshly formed capsules. This value decreased by another 8% when the sample was 12 days old but did not change when the sample aged for 25 days. This change in thermal conductivity with sample aging is consistent with an increased oxide shell thickness demonstrated by Farrell et al.[82] (*i.e.*, an increased volume fraction of low thermal conductivity oxide in the capsule bed).

The pressure required to reach the peak conductivity was not impacted significantly by the sample age. Figure 2.4 shows how the value of the average peak thermal conductivity and the corresponding pressure changed with sample age. The measurements reveal that capsule age must be taken into consideration during the design of LM filler-based composites.

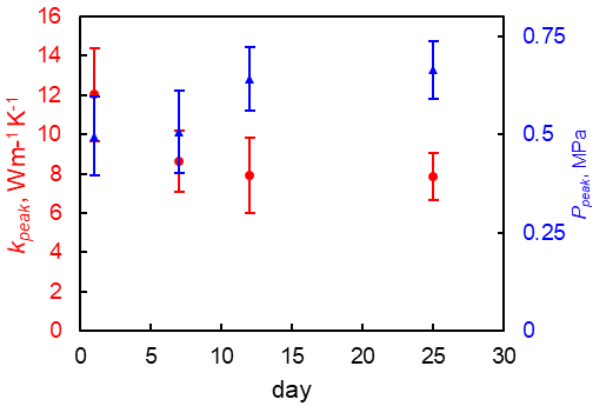

Figure 2.4: Plot showing the impact of the oxide shell aging on the average peak thermal conductivity (k_{peak}) and corresponding pressure (P_{peak}) for beds consisting of LM capsules with an average diameter of 6.6 ± 1.6 μm.[87]

2.4.2 Capsule Diameter

In order to characterize how the average capsule diameter impacts the capsule rupture process, I fabricated LM capsules with average diameters of 0.7 ± 0.5, 1.4 ± 0.6,

3.1± 0.8, and 6.6 ± 1.6 μm. The change in their thermal conductivity as a function of pressure was measured to obtain the peak thermal conductivity and corresponding pressures. All samples were aged for 7 days due to the multi-day sedimentation process required to isolate 0.7 μm diameter LM capsules.

The data reveals that increasing the LM capsule diameter increases the thermal conductivity, which is also consistent with a decreased volume fraction of low thermal conductivity. It is also evident from the data that larger capsules ruptured more easily and that the rupture pressure scales as d^{-1}. Figure 2.5 shows the highest thermal conductivity of over 8 W m^{-1} K^{-1} is obtained for the 6.6 μm average diameter capsules at a P_{peak} of around 0.5 MPa while that of the bed consisting of 3.1 μm average diameter capsules resulted in a mildly lower k_{peak} of over 6 W m^{-1} K^{-1} at a P_{peak} of around 1 MPa.

In contrast, compression of the bed consisting of 1.4 μm average diameter capsules resulted in a k_{peak} of around 5 W m^{-1} K^{-1}, but required a P_{peak} of over 1.5 MPa, while compression of the bed consisting of the 0.7 μm average diameter capsules resulted in a k_{peak} of only 3 W m^{-1} K^{-1} and more than a doubling of P_{peak} to over 3 MPa (0.7 μm diameter capsules did not rupture even after the experimental system's highest pressure had been applied as illustrated by the inset SEM image in Figure 2.5). Evidently, increasing the average capsule diameter above a few micrometers dramatically facilitates the shell rupturing process within the bed.

Interestingly, the P_{peak} and average capsule diameter (d) from the thermal results follows the same scaling relation between the pressure and diameter of a spherical thin-walled pressure vessel, *i.e.*, $P = 4\sigma t d^{-1}$ where σ is wall stress and t is the wall

thickness. Assuming the fabricated LM capsules as spherical thin-walled pressure vessels, and using tensile strength and thickness of the gallium oxide shell, which have been reported to be 1 GPa[88] and 2.2 nm[82], I estimate coefficient of $4\sigma t$ = 8.8 N m^{-1} for the d^{-1} scaling. Using the experimental data, I fit the P_{peak} data trend to a simple inverse relationship of $P_{peak} \sim cd^{-1}$, where *c* is a scaling factor as shown in Figure 2.5c. The experimental data provides value of *c* as 2.52 ± 1.5 N m^{-1} based on uncertainty weighted fit. Even though the value of this scaling factor does not exactly match with the $4\sigma t$ estimated theoretical coefficient, these are of the same order magnitude. The mismatch is attributed to the complex nature of the rupture mechanics of thin oxide shells in a LM capsule bed under compression, compared to the simple thin-walled pressure vessel theory.[64,89,90] The inverse dependence of pressure on capsule diameter noted here in this work is consistent with the work of Boley *et al.*[64] They found that the force per capsule required for rupturing, *f*, was linearly proportional to the capsule diameter, *d*, or $f \sim d$. This relation can be rearranged in terms of rupture pressure as $P \sim f/d^2 \sim 1/d$, which is the general d^{-1} scaling explained above (see Appendix A, figure A2).

The data for P_{peak} is compared with electrical conductivity onset pressures in Figure 2.5b and even though the trend matches for the thermal and electrical conductivity onset pressure, there is a clear offset for the thermal onset pressure. The thermal onset pressure is higher than the electrical values. This highlights that for achieving high thermal conductivity, sufficient pressure needs to be applied to rupture the oxides and achieve numerous percolation pathways, which is higher than that required for the onset of electrical conductivity.

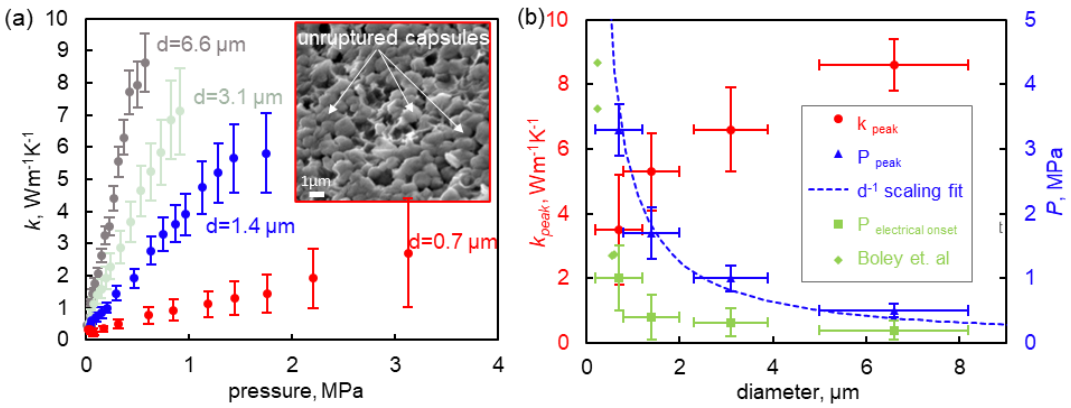

Figure 2.5: (a) Plot showing the thermal conductivity (k) of LM capsule beds as a function of applied pressure for varying diameters of LM capsules. The capsules in these experiments were all 7 days old. The inset shows that not all of the LM capsules ruptured for the smallest size distribution even after the upper pressure limit was applied by the measurement system. (b) k_{peak} and P_{peak} data along with the pressure required for the onset of electrical transport from the experiments in this work (green squares) and the work of Boley et al.[64](green diamonds).[87]

2.4.3 Chemical Treatment

In order to facilitate the oxide shell rupture process, I chemically treat the LM capsules with dodecanethiol (DDT) and HCl since this leads to modification of the capsule properties.[62,70,82,86]. DDT binds to gallium sites via the thiol group, hinders the oxide formation, and stabilizes the structure of LM capsules even if treated with HCl acid.[86] In contrast, untreated LM capsules immediately coalesce into a bulk droplet when treated with HCl. Hence, a combined treatment of dodecanethiol and HCl acid has the potential to create stable LM microcapsules with significantly degraded (*i.e.*, weakened) oxide shells.

For this evaluation, I use three sets of freshly prepared LM capsule samples of an average diameter of about 8 µm. The first set of samples is the untreated LM capsules that are used for the control experiment (gray data in Figure 2.6). The second set of

samples are prepared using DDT to obtain LM capsules with thiol-modified oxide (red data in Figure 2.6). The third set of samples is prepared using DDT and additionally treated with HCl acid. (blue data in Figure 2.6).

The plot in Figure 2.6 shows that out of the three sets of samples, the DDT+ HCl acid treated samples show the highest thermal conductivity of 16 W m^{-1} K^{-1} at a low P_{peak} of less than 0.2 MPa. The untreated capsules achieved a k_{peak} of 12 W m^{-1} K^{-1} at a P_{peak} of around 0.4 MPa. This result suggests that the dilute HCl solution successfully degrades the oxide shell, and that the thiol may prevent, or at least delay oxide regrowth. The addition of the dilute HCl treatment after thiolation strongly facilitates the rupturing process. The effect of this treatment is also substantial: relative to untreated capsules, the thermal conductivity increases by a third and requires only half the rupture pressure.

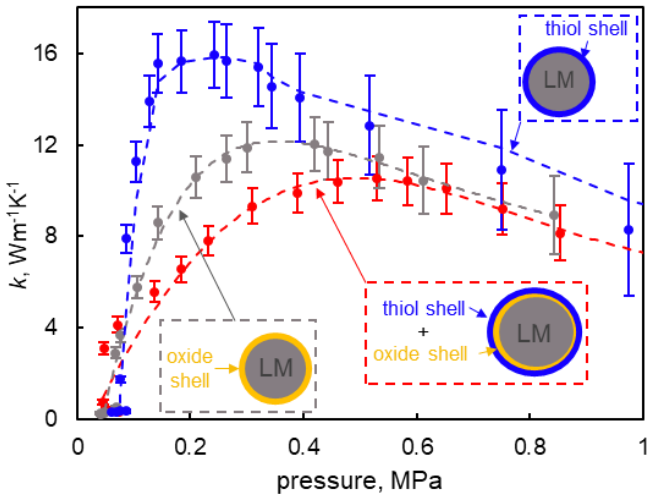

Figure 2.6: Thermal conductivity of LM capsule beds as a function of the applied compressive pressure for varying chemical treatments on the oxide shell of the capsule. Data are shown for untreated LM capsules (control experiment, gray data), dodecanethiol-treated capsules (red data), and dodecanethiol-treated capsules followed by a dilute HCl acid treatment (blue data). The LM capsules in these experiments have an average diameter of 8 μm and are freshly prepared (*i.e.*, data taken on day 1).[87]

The increased thermal conductivity and decreased rupture pressure accompanying chemical functionalization are favorable with respect to TIM performance. However, the change in rupture pressure is particularly important because of two reasons. One, microelectronics packaging has constraints for pressure, and typical pressure values are on the order of 25 psi (0.172 MPa).[91] The rupture pressure of 0.2 MPa obtained in this work for chemically treated LM capsules approximately matches this value and hence represents a meaningful accomplishment. Second, the matrix resistance will influence the pressure required to achieve particle connectivity by introducing the matrix between the fillers. This reduction in pressure due to the weakening of the oxide layer at filler level will help form connectivity in a polymer matrix.

2.5 Conclusions

In this chapter, I provide insights into the fundamentals of oxide rupture mechanics in LM capsules. To achieve maximum thermal transport, majority of LM capsules need to be ruptured. This leads to the formation of numerous thermal percolation pathways and a significant increase in the thermal conductivity can be obtained. Further, this work identifies the critical parameters of LM that impact the oxide rupture, namely LM capsule age, size distribution and oxide shell chemical treatment, and their implications on the functional properties of LM capsules is quantified. Freshly prepared capsules yield highest thermal conductivity and increasing the LM capsule diameter further increases the thermal conductivity. In addition, chemical modification can be adopted to modify and weaken the oxide shell which facilitates its rupture. The capsules

treated with dodecanethiol and hydrochloric acid achieved a thermal conductivity of 16 $W\ m^{-1}\ K^{-1}$ at a pressure below 0.2 MPa. Importantly, this pressure is well within the range acceptable for TIM applications.

However, the introduction of a polymer matrix will add additional thermal resistance paths that will prevent the bridging of the LM capsules. The next Chapter will discuss the factors that hinder the LM capsules bridging in a polymer matrix and shed light on the mechanisms as well as identify the additional controlling knobs that can assist in enhancing thermal transport in polymer composites.

CHAPTER 3

3. BRIDGING LIQUID METAL FILLERS WITH REACTIVE MEAL CO-FILLERS AND MATRIX TUNING

3.1 Introduction

Chapter 2 discussed how rupturing the oxide shell reduces the interfacial resistance between the LM capsules and forms a thermal percolation network in a LM capsule bed only. In this chapter, I introduce uncured polymer matrix and discuss the thermal transport barriers in a LM polymer composite with uncured matrix and demonstrate a path to overcome them. Here, I identify the various knobs like filler type, volume fraction, matrix viscosity, and filler processing that can be used to tune the thermal and mechanical properties of LM-based polymer composites.

As discussed previously, limited investigations have been done with LM fillers in a polymer matrix from a thermal application perspective. The following sections will discuss the reasons for limited thermal conductivity improvement and elaborate on the mechanisms underlying the experimental trends obtained for the LM filler-based composites.

3.2 Multiphase Composite System

3.2.1 Filler-Matrix interaction

The addition of LM fillers in silicone oil matrix has shown limited improvement in the polymer composite thermal conductivity.[92] Based on the revelations of the oxide rupture mechanism on thermal transport discussed in the previous chapter, the direct

mixing approach resulting in low thermal conductivity can be attributed to two major factors. First, the introduction of matrix does not allow the LM fillers to come in direct contact. Second, the LM oxide shells do not rupture effectively.

To overcome these thermal impediments, I introduce solid metal co-fillers into the composite system along with polymer matrix with different viscosities. In this work, silver (Ag) is used as the solid additive because it rapidly alloys with gallium to form anisotropic needle-like crystals that could act as additional thermal pathways that assist in rupturing the oxide shell of LM fillers as illustrated in Figure 3.1.

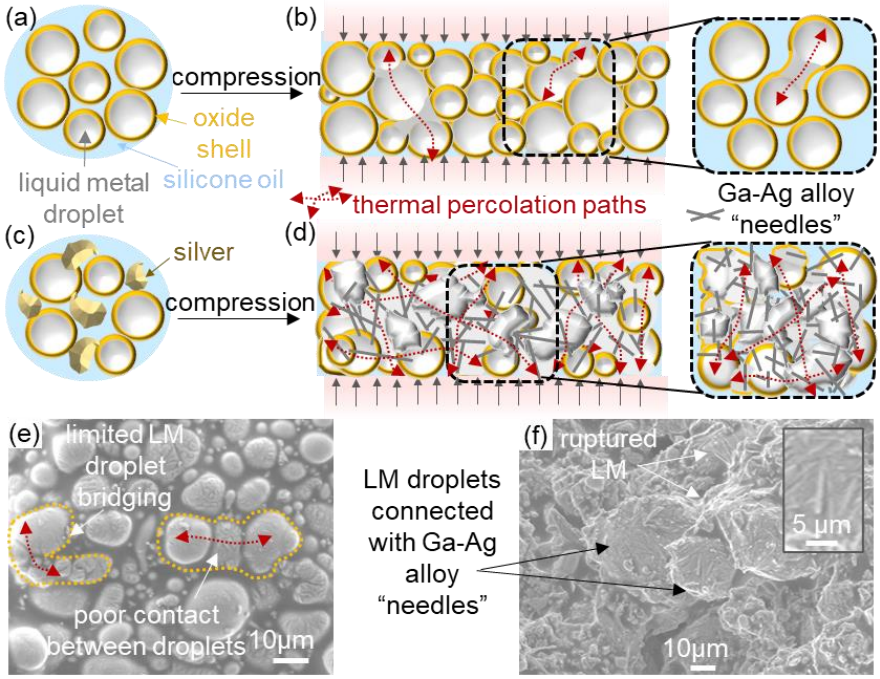

Figure 3.1: Schematics showing (a) LM droplet−silicone oil composite and (b) formation of a few percolation pathways across it during substantial compression, (c) silicone oil composite with solid (Ag) and liquid (Ga) fillers, and (d) formation of multiple percolation pathways through pressure and Ga−Ag alloying induced bridging of LM droplets; SEM micrograph showing an example of (e) poor contact between LM droplets and rare droplet bridging in silicone oil matrix after substantial compression (≥4 MPa) and (f) formation of numerous Ga−Ag intermetallic alloy needles in Ga−Ag silicone oil composite after substantial compression (≥4 MPa).[93]

3.2.2 Fabrication of Multiphase Composite

LM droplets (diameter 5.4 ± 1.3 μm) were fabricated from pure gallium (Rotometals) through ultrasonication followed by sedimentation, as discussed in the previous chapter.[87] Commercially available Ag powder (Alfa Aesar, diameter 1.3± 0.6 μm) was used as solid additive. To prevent a priori alloying of silver and gallium, the fillers were sequentially mixed in the silicone oil (Sigma-Aldrich). In order to demonstrate the role of polymer rheology in the formation of thermal network, different viscosities (10 cSt, 100 cSt, and 1000 cSt) of silicone oil were used for this work. Further, all the composites were made with a total filler volume fraction of 50% which is known to be the percolation threshold for spherical particles.[32,34] Fixing the total filler ratio, this work further discusses the importance of filler composition tuning by varying the ratio of LM to Ag to get the desired thermal enhancement. This is discussed in detail in the next section.

3.3 Thermal Enhancement Design Knobs

3.3.1 Tuning Filler Ratio

The LM:Ag filler volume ratios were selected based on the Ga atomic percentage. In particular, I have utilized 15%, 30%, 47%, 57%, 70%, and 80% Ga atomic percent which translates to Ga:Ag:Silicone oil volumetric ratios of 8:42:50, 17:33:50, 25:25:50, 30:20:50, 37:13:50, and 41:9:50, respectively. The composites with these ratios were fabricated for the three different silicone oil viscosities. These were then characterized on the SBA setup as discussed in chapter 1.

Through this evaluation, the main impact identified is that LM and solid filler ratio need to be tuned to get the desired functional properties. There is a proper balance between the presence of unreacted liquid metal and sufficient formation of alloy needles to obtain a peak in the thermal conductivity. This is obtained for 70at% Ga for which the Ga:Ag:Silicone Oil is 37:13:50 v/v. The maximum effective thermal conductivity k_{eff} obtained at this ratio is 21 W m^{-1} K^{-1} for 2.2 mm thick samples which increases to 25 W m^{-1} K^{-1} as the sample is compressed to 4 MPa in the 10 cSt silicone oil matrix as shown in Figure 3.2. The k_{eff} of the silver only samples show the highest values for 4 MPa pressure. However, these Ag-only samples compact into highly porous "cakes" that crumble too easily for any practical applications (see Appendix B, figure B1).

The data illustrates another important aspect of the thermal transport mechanism when the filler ratio changes from 100 at% Ga (only Ga in silicone oil) to 80 at% Ga. A sharp increase in thermal conductivity highlights that even a small fraction of solid Ag particles strongly assists in creating additional thermal pathways via the Ga-Ag intermetallic alloy "needle" formulation. However, the thermal conductivity gradually reduces with the addition of more silver *i.e.*, reduction in Ga at%. For the 10 cSt silicone oil-based samples, with 2.2 mm thick sample the k_{eff} drops to 5 W m^{-1} K^{-1} as the Ag is increased and gallium is reduced to 15 at% Ga. This is due to the gradual depletion of unreacted LM and domination of the sample composition by solid Ga-Ag alloy and pure Ag agglomerates (see Appendix B, figure B2) that display high particle-particle contact resistance which is detrimental to the thermal transport in-between particles.

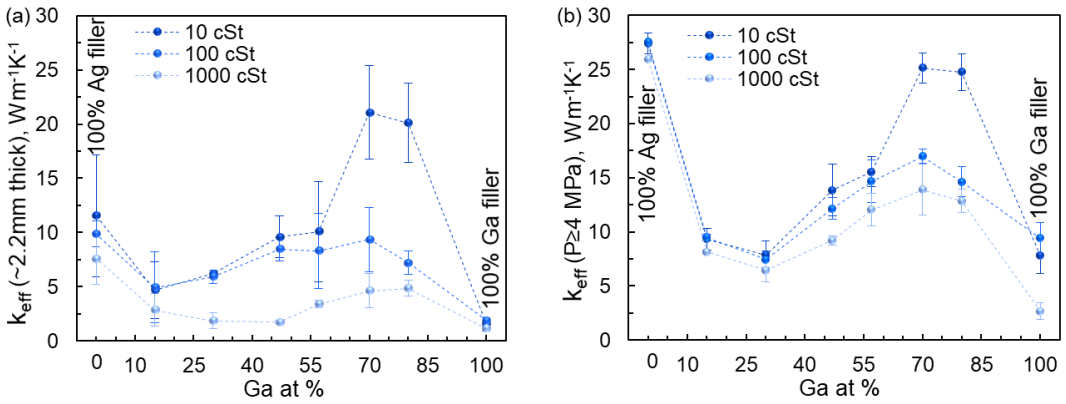

Figure 3.2: (a) Effective thermal conductivity of composite samples with varied Ga:Ag ratio in a constant 50% volume fraction of silicone oil at a constant sample thickness of about 2.2 mm, (d) Effective thermal conductivity of composite samples with varied Ga:Ag ratio in a constant 50% volume fraction of silicone oil at a pressure of ≥4 MPa.[93]

In addition to the liquid filler:solid metal fraction, the silicone oil viscosity also has a very pronounced impact on the k_{eff} of the composites. The magnitude of change in the k_{eff} due to oil viscosity is the strongest at 70-80 at% Ga. Quantitatively, as the viscosity is decreased from 1000 cSt to 100 cSt at 70at% Ga for 2.2mm thick samples, the k_{eff} increases from 4.6 W m^{-1} K^{-1} to 9.3 W m^{-1} K^{-1} and even more substantially to 21 W m^{-1} K^{-1} upon reducing the viscosity to 10cSt. This highlights that the formation of thermally conducting pathways is also a function of polymer rheology.

The following section discusses the impact of pressure on the thermal conductivity of these polymer composites.

3.3.2 Role of Pressure

Similar to chapter 2, which revealed compression-induced oxide shell rupture and formation of thermal percolation pathways, here I employ compression to understand the underlying mechanisms that can help enhance the thermal conductivity when a polymer matrix is introduced. This work reveals that the thermal conductivity of LM-based

polymer composites can be enhanced if the matrix is displaced effectively from between the filler particles, particles come in direct contact and alloy, oxide ruptures, and thermal bridging occurs. For all these mechanisms to activate, it is critical to understand the impact of pressure on the effective thermal conductivity of the composites. The variation of k_{eff} with pressure for composites with 50 vol% 100 cSt silicone oil for different Ga at% is shown in Figure 3.3 (trend of effective thermal conductivity with pressure for different compositions shown in Appendix B, Figure B3).

Under compression, the 100 at% Ga, *i.e.*, only Ga filler) composite shows a similar trend as observed for LM capsule beds in the "air matrix". The k_{eff} increases rapidly at low pressure when over 90% of the sample is squeezed, most of the matrix is displaced bringing the LM particles closer in contact. On further compressing the sample, the k_{eff} peaks and decreases due to the widespread rupturing of LM particles and some sample leakage.[87] However, the incorporation of even a small amount of Ag particles mostly eliminates this non-linear trend of k_{eff} with pressure. As seen from Figure 3.3, the k_{eff} increases nearly linearly with pressure for most samples and some saturation is observed under high pressure. The slope of this trend increases as the Ag particle fraction increases.

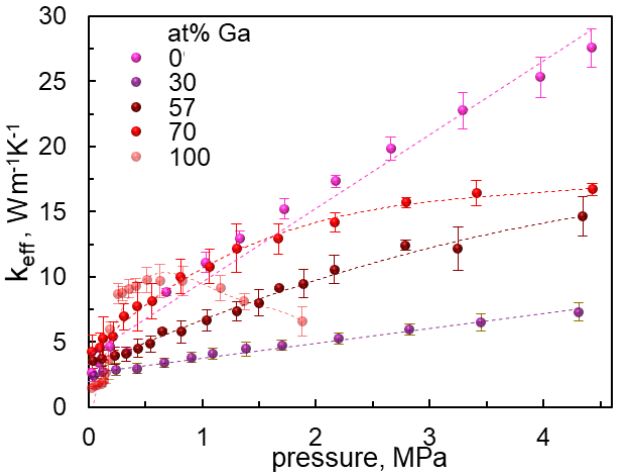

Figure 3.3: Impact of pressure on thermal conductivity of 100 cSt silicone oil based composites for different Ga at% in 50 vol % silicone oil[93]

The contact resistance of composites is another important parameter that impacts the effective thermal conductivity of TIMs. To determine the intrinsic thermal conductivity of the composite, the 70 at% Ga in 50 vol% 100 cSt silicone oil was used. The contact resistance was decoupled by using the thermal resistance measurements as a function of the sample thickness. This was done for different pressures and the intrinsic thermal conductivity was obtained by taking the inverse of the slope in Figure 3.4a. The values tabulated in Table 3.1 show the significance of pressure on the contact resistance, reducing by 15% when the pressure increases from 2 MPa to 4 MPa.

An important aspect of sample fabrication is revealed through this data and shows how pressure can be used as an activation mechanism to fabricate high conductivity polymer composites.

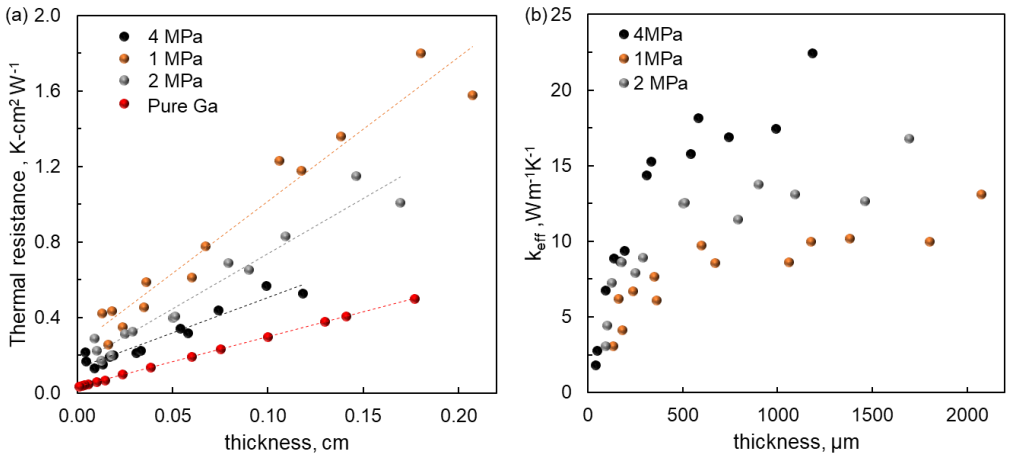

Figure 3.4: (a)Thermal resistance and (b)effective thermal conductivity vs. sample thickness data for the LM:Ag:Silicone oil composite with 70% atomic fraction of gallium measured at varied pressures[93]

Table 3.1: Intrinsic thermal conductivity and thermal contact resistance for LM-Ag polymer composite in 100 cSt silicone oil matrix

	Pressure, MPa	Intrinsic thermal conductivity, K_{bulk} W $m^{-1}K^{-1}$	Contact resistance, K cm^2 W^{-1}
100 cSt, 70at% Ga	1	13.1	0.254
	2	17.1	0.154
	4	26.7	0.131
Pure Ga		37.0	0.016

3.3.3 Role of Matrix Viscosity and Filler Processing in Thermal Bridging

The increasing thermal conductivity obtained with a decrease in the viscosity of the oil matrix is further investigated to understand the underlying mechanism dictating the thermal boost that is obtained in the composite samples.

An alternate filler fabrication technique of pre-mixing fillers was employed, and the thermal conductivity and morphology of the samples was studied. Specifically, the

Ag particles were first mixed with LM droplets and then these pre-mixed fillers were added to the oil matrix. This way the mechanism of Ga-Ag alloying with “needle” formation is decoupled from the impact of the oil matrix. These pre-mixed samples when compressed to 4 MPa have a k_{eff} of 25 W m^{-1} K^{-1}, irrelevant of the oil viscosity (Figure 3.5b). This value closely matches the case of “no oil” and 10 cSt oil samples with sequentially mixed samples which shows that the 10 cSt silicone oil matrix does not pose much more of a physical barrier than air.

Direct contact of the filler particles, breaking of the oxide and the Ga-Ag alloying happens easily with an “air matrix” as well as 10 cSt silicone oil matrix. This can occur only if the oil drains sufficiently from in-between the filler particles to enable their physical contact.

Thus, these results explain the thermal bridging mechanism in the presence of matrix with different viscosities. The lower viscosity oils can effectively drain from in-between the filler during compression and allow for the formation of multiple percolation pathways enabled by rupturing the oxide shell as well as with the formation of the Ga-Ag alloy needles (Figure 3.5a). More viscous oils inhibit these thermally beneficial processes because they cannot fully drain and are partially trapped in-between the filler particles.

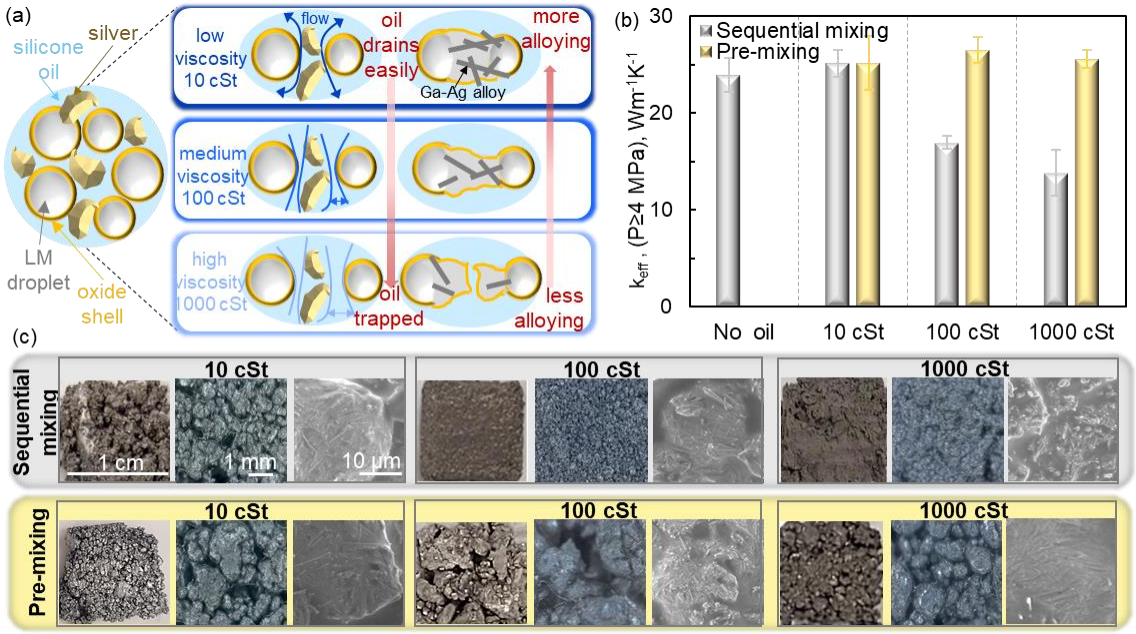

Figure 3.5: (a) Schematic illustrating how lower viscosity of the matrix of Ga−Ag−silicone oil composite drains easier and enables more Ga−Ag alloy formation; (b) bar plot showing the effect of premixing fillers on effective thermal conductivity of Ga:Ag: silicone oil composites with 70 at% Ga and 50 vol % silicone oil, (c) multiscale optical and SEM images of the composites with the sequentially mixed and the premixed fillers as well as 10 cSt, 100 cSt, and 1000 cSt silicone oil matrices (the scale bars in all the image triplets are same as indicated in the upper left image set)[93]

The morphology of the pre-mixed, sequentially mixed samples for different oil viscosities further supports the “oil draining” mechanism. Macroscopically, the pre-mixed samples for all oil viscosities and the 10 cSt sequentially mixed samples show formation of large globules. The SEM images in Figure 20c show the presence of numerous alloy needles. The large clumps predominantly consist of particles, between which abundant alloying has occurred. The sequentially mixed filler samples for 100 cSt and 1000 cSt show a more homogeneous distribution of fillers. The extent of alloying is considerably less than the pre-mixed filler samples or 10 cSt sequentially mixed samples.

The large Ga-Ag clusters provide efficient thermal pathways across the composites and enhance their thermal conductivity.

High thermal conductivity is one of the design considerations of polymer composites. To be suitable for practical applications like a TIM candidate, the composites should also have the desired mechanical properties of compliance, macroscopic homogeneity, ease of application, etc., as was discussed in chapter 1. The next section discusses the mechanical characteristics of the composites.

3.4 Mechanical Design Parameters

3.4.1 Compression Characteristics

The compressibility of different formulations gives insights into the compliance characteristics of the polymer composites. The samples containing only LM are highly compressible even at low pressures with the 100 at% Ga showing 93% compression at 0.5 MPa (Figure 3.6a). With the incorporation of even a small amount of silver, the composite stiffens, and the compression obtained for 70 at% Ga is ~60% at 3 MPa. Further increase in the silver fraction has more gradual mechanical effects with the 0 at% Ga *i.e.,* full silver sample showing only ~35% compression at 3 MPa.

The thermal conductivity obtained for pre-mixed filler samples is superior to the sequentially mixed samples. Comparison of their compression characteristics shows that the pre-mixed filler composites have lower compression of ~45% at 3 MPa compared to the sequentially mixed fillers with ~60% compression at 3 MPa (Figure 3.6b)

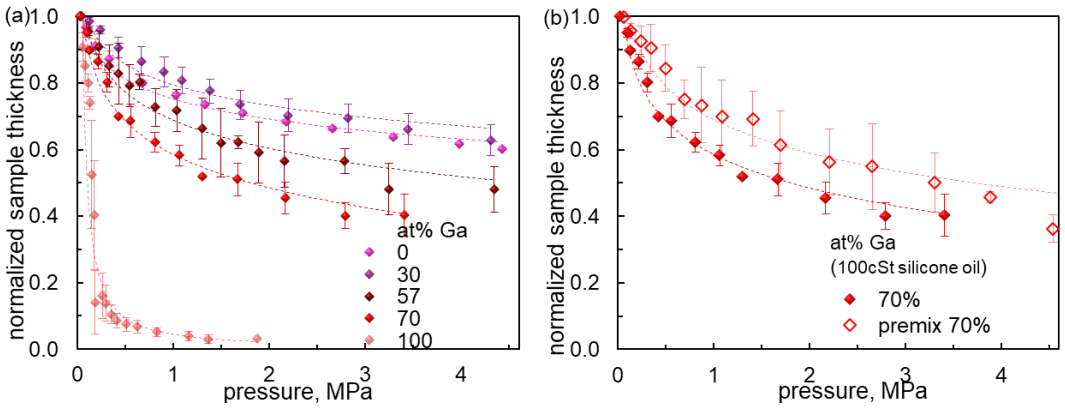

Figure 3.6: Variation of composite thickness (normalized to initial thickness of each sample) with application of pressure for composites with fillers in 50 vol% 100cSt silicone oil for (a) Different Ga at% and, (b) pre-mixed and sequentially mixed filler samples for 70 at% Ga [93]

The balance between thermal and mechanical characteristics is evident in Figure 3.7 which shows the microscopic features of 30 at% Ga, 70 at% Ga sequentially mixed fillers and 70 at% Ga with pre-mixed filler. As shown in the previous sections the 30 at% Ga has low thermal conductivity (7.5 W m^{-1} K^{-1}) compared to the 70 at% Ga composition (17 W m^{-1} K^{-1} when sequentially mixed, 26.5 W m^{-1} K^{-1} with pre-mixing fillers). This is also explained by the SEM micrographs which show limited Ga-Ag alloy formation clustered in a localized region of the sample. These composites have unreacted silver as seen from Figure 3.7a and this causes the compressibility of the samples to be also low (~30% at 3 MPa).

For the fixed 70 at% Ga composition, the pre-mixed filler samples have densely populated Ga-Ag alloy needles and ruptured LM is seen connected in the sample which explains the high thermal conductivity. However, the compression characteristics of the pre-mixed fillers are inferior (35% compression at 3 MPa) to the sequentially mixed filler samples (~60% compression at 3 MPa). Also, the presence of large clumps originating

from the filler premixing is not desirable for TIM applications. The next section gives details on the macroscopic structure of the various compositions explored in this work.

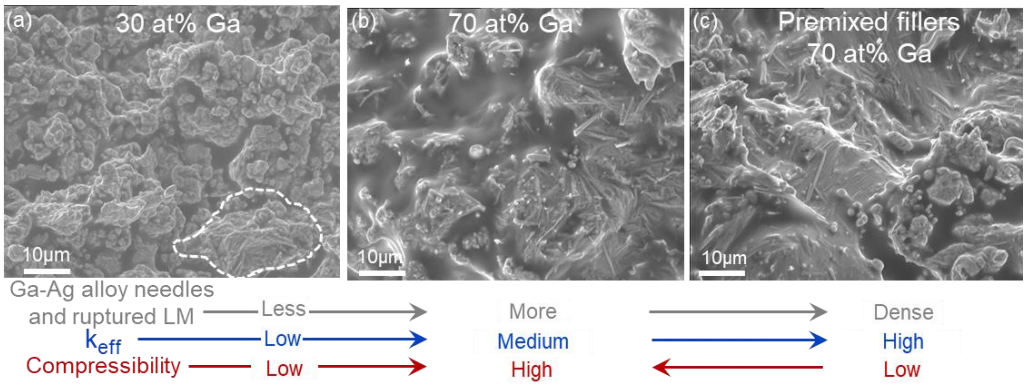

Figure 3.7: SEM micrograph showing formation of Ga−Ag intermetallic alloy in composite after substantial compression (≥4 MPa) for different ratios of Ga:Ag:silicone oil in 100 cSt oil (a) 30 at% Ga (17:33:50 v/v), (b) 70 at% Ga (37:13:50 v/v), and (c) premixed fillers at 70 at% Ga.[93]

3.4.2 Macroscopic Homogeneity

The macroscopic morphology of polymer composites is another factor that is considered for identifying potential candidates for practical application like TIM in this case. All the 1000 cSt composites have predominantly powder-like consistency that can create unacceptable large air voids. For the 10 cSt samples, the gallium-rich composites (70 at% Ga and 80 at% Ga) have large clusters and are powder-like in nature. Amongst the 100 cSt silicone oil viscosity samples, the highlighted 70 at% Ga composite in Figure 3.8 gives the highest effective thermal conductivity of 17 W m^{-1} K^{-1} at 4 MPa. This value is a function of the pressure and drops to 14 W $m^{-1}K^{-1}$ and 10.8 W $m^{-1}K^{-1}$ when the pressure is decreased to 2 MPa and 1 MPa, respectively. By removing the contact resistance, the intrinsic thermal conductivity was extracted as 26.7 W m^{-1} K^{-1}. The inclusion of LM fillers in polymers has resulted in composites with thermal conductivity

of 4.8-6.7 W m^{-1} K^{-1}, which increases to ~11-17.6 W m^{-1} K^{-1} upon applying directional strain.[36,60] Without applying high strain, the value of LM composites can be increased to 9.9 W m^{-1} K^{-1} by including hybrid liquid metal-coated silicon carbide particles.[56] Thus, the composites with silver and LM particles with optimized silicone viscosity provide excellent thermal conductivity.

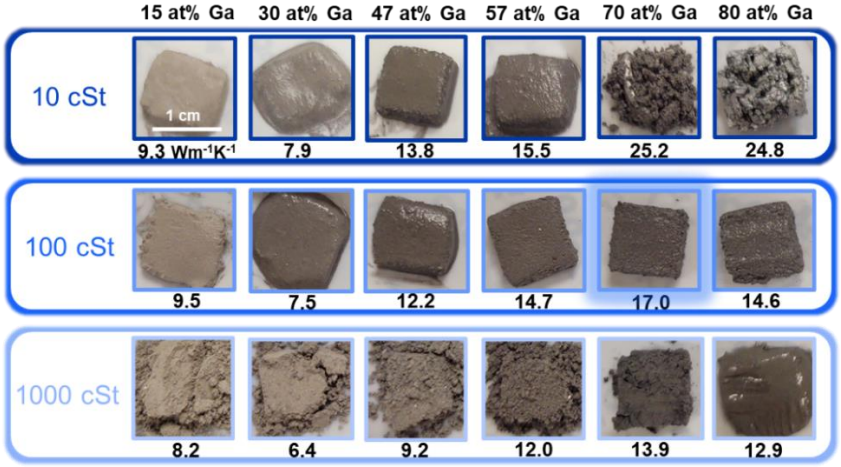

Figure 3.8: Images of all the studied LM:Ag:Silicone oil composites demonstrating their macroscopic morphology and thermal conductivity.[93]

3.5 Conclusions

Understanding the design parameters of polymer composites like polymer viscosity, filler composition, pressure for thermal percolation, filler fabrication technique, and mechanical compliance is the key to developing future highly conducting LM-based cured polymer pads. In addition, these insights can be further extended in developing polymer composites with tunable properties for other applications like sensors, wearables and soft conductors. The thermal and morphological characterization of the Ga-Ag fillers in uncured polymer illustrated in this chapter reveal the dominant roles that the matrix viscosity and filler ratio have on the composites. Specifically, the higher viscosity of

1000 cSt oil inhibits the physical contact between the fillers during the sample compression, which the 10 cSt oil can overcome through its ability to drain from in-between the particles effectively. However, it is not just enough to tune the matrix viscosity as it does not lead to a substantial thermal boost. Thus, solid additives like Ag are required to ensure the LM oxide shell ruptures. This alloy-assisted popping of LM also connects the LM fillers within the matrix and act as thermal anchors. Striking a balance between thermal and mechanical properties is critical. Knobs like pre-mixing fillers provide sufficient thermal bridging in composite to enhance the heat transport but render macroscopic non-homogeneity in the composites by the formation of clumps which is undesirable.

The next critical step is translating the identified design knobs to develop composites with cured polymer matrix as discussed in the next chapter.

CHAPTER 4

4. COMPRESSION-ACTIVATED MULTI-PHASE FILLER NETWORKS IN ELASTOMERS BY MODULATING PRE-CURE MATRIX VISCOSITY

4.1 Introduction

In this chapter, I introduce a multipronged strategy to generate polymer TIM pads with enhanced thermal conductivities. In this strategy, I integrate the thrusts of the previous chapters, *i.e.*, employing multi-phase fillers, tuning the polymer matrix pre-cure viscosity, and using mechanical compression during sample curing. This work reveals that the interfacial interaction between fillers, polymer matrix, and formation of thermal networks needs to be achieved pre-curing of the polymer pad and can be preserved by employing in-situ external stimuli of compression to activate the thermal pathways.

This approach builds on the insights of chapters 2 and 3, that the oxide shell of LM droplets ruptures easily for droplets that are freshly prepared and are microscale, and that the introduction of solid Ag particles that react with Ga substantially facilitate thermal bridging across the multi-phase fillers. The liquid and solid fillers spontaneously react with each other to form intermetallic alloys. These intermetallic alloys crystallize into high aspect-ratio solids (*i.e.*, nanoneedles) that improve thermal percolation. Further, the uncured polymer matrix with low viscosity (~100 cSt silicone oil), enhances thermal conductivity by facilitating oil displacement from in-between the particles during compression. The high viscosity silicone oils of ~1000 cSt inhibit the filler-filler contact within a compressed uncured polymer matrix and results in a lower conductivity.

Through this work, I demonstrate that this polymer rheology dependency of efficiently forming multiple thermal percolation pathways is an important factor because many of the precursor polymer solutions that are commonly used for solid-phase TIM pads(*e.g.*, Sylgard 184 and Ecoflexes[94,95]) have an even higher pre-cure viscosity of around 2,000-5,000 cSt.[96] I introduce the use of a tailored silicone polymer precursor solution system that can have pre-cure viscosities of ~100 cSt and ~2,300 cSt. Employing these two silicones, I show that all the highly thermally beneficial features can be preserved within a cured solid-phase TIM pad.

4.2 Fabrication of Composites with Tuned Pre-Cure Matrix Viscosity

4.2.1 Mixing Methodology of Constituents Pre-Curing

The TIM pad fabrication process in this work consists of preparing Ga LM micro-droplets with controlled size distribution through ultrasonication and selective sedimentation.[93,97], formulation of a precursor polymer solution, sequential mixing of reactive solid co-fillers, and subsequent thermal curing under applied load. Integrating the identified parameter of size of LM filler from chapter 2, in order to promote facile rupture of the LM oxide shell on the droplets, I adjusted the ultrasonication and sedimentation time to obtain LM droplets with a diameter of 8.2 ± 4.2 μm (68% confidence interval).[97] Commercially available Ag powder (Alfa Aesar, APS 4-7 μm particle size)is used as the solid metal additive (see Appendix C, Figure C1 for SEM images illustrating the size and shape of the Ga and Ag fillers)

To tune the precursor polymer solution viscosity, this work uses a vinyl-terminated polydimethylsiloxane (V-PDMS) elastomer system available from Gelest Inc to create the polymer matrices with pre-cure viscosities of ~100 cSt and ~2,300 cSt. This elastomer system has five components (adjustable base polymer, crosslinker, inhibitor, catalyst, and chain extender) that can be chosen to vary the resultant properties.[94,98] The base polymer and chain extender are available in a wide range of viscosities (we use 100 cSt and 3,500 cSt base polymer). The pre-and post-cure mechanical properties of these silicones are also influenced by the molar ratio of the crosslinker and chain extender (greater than 0.2 is recommended[94], and we use 0.56 in this work) and the molar ratio of the crosslinker to the polymer base (less than one is recommended[94] and we use 0.78 in this work). The V-PDMS "part A" consists of a base polymer, catalyst, and inhibitor, while the V-PDMS "part B" consists of a crosslinker and chain extender. To yield the ~100 cSt pre-curing viscosity of the precursor polymer solution, DMS-V21 is used as the base polymer, SIP6830.3 platinum catalyst, and SIT7900.0 inhibitor to formulate "part A" and DMS-H21 chain extender mixed with HMS-301 crosslinker to formulate "part B". To yield the ~2,300 cSt pre-curing viscosity of the precursor polymer solution, the base polymer in "part A" is substituted with DMS-V33. The pre-curing viscosity was measured using a rheometer (see Appendix C, Figure C2).

It is important to note that V-PDMS formulation was mixed sequentially in parts. The Ga LM and Ag fillers were sequentially mixed into the V-PDMS formulations (see schematic in Figure 4.1) to minimize premature alloying between the LM and Ag prior to sample curing under applied load. Specifically, first, the newly fabricated LM droplets

were gently mixed into the "part A" of the V-PDMS. This covers the LM droplets in a precursor polymer solution coating that decreases direct contact, and hence alloying, between the LM and any subsequentially-added Ag filler particles. For composites with combined LM and solid particle additives, the Ag particles were then stirred into "part A" of the V-PDMS. "Part B" was then added to the precursor polymer solution.

All the composites were fabricated with a total filler volume fraction of 50%, which is known to be above the percolation threshold for spherical particles.[13,32,34,99] For composites with both solid and liquid fillers, the selection of LM:Ag ratio was selected on the basis of Ga atomic percentage (at%) that yields the highest thermal conductivity in silicone greases that is discussed in chapter 3.[73] Specifically, the ratio was fixed at 70 at% Ga, which translates to a composite of Ga:Ag:silicone elastomer volumetric ratio of 37:13:50[93] (corresponding to 0.7 g Ga fillers, 0.46 g Ag particles, and 0.16 g of precursor polymer solution).

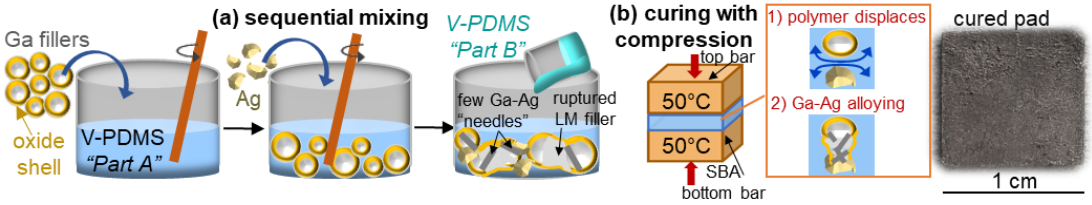

Figure 4.1: Schematical depiction of the composite polymer pad fabrication: **(a)** the sequential Ga and Ag filler mixing with parts A and B of the V-PDMS and **(b)** the thermal curing of the pads under varying levels of compression. The applied pressure during curing displaces the uncured precursor polymer from in-between filler particles. Upon direct contact, the Ag and Ga fillers react to form intermetallic alloy particles with a needle-like shape. Also illustrated is a photograph of an ~1 cm x 1 cm cured pad.

It is important to note that some contact and alloying between the LM and Ag[93] occurs during the mixing process and that the extent of this contact is higher in the lower

viscosity matrix. However, in either matrix, the degree of alloying during the mixing process is minimal compared to the alloying induced by compression during curing. This is evidenced by a significant increase in thermal conductivity for samples with applied curing pressure relative to those without applied curing pressure, which is discussed in the following sections.

4.2.2 Curing Process Parameters

After the uncured polymer composite sample was formulated, the curing process was carried out in the variable-pressure thermal conductivity measurement system (SBA)[72] that is based on a modified ASTM D5470 standard[100] as discussed in chapter 2. The sample was loaded into the system by placing it between upper and lower copper reference bars with a known cross-sectional area[73,75,101] and pressure during curing was applied. The copper reference bars are equipped with a linear encoder and load cell that determine sample thickness and applied pressure. The copper bars are also equipped with a heater and thermocouples to apply heat and measure temperature.

To cure the sample under applied load, a sliding sample mold was placed around the lower copper reference bar in the SBA and the uncured sample was transferred into the mold. In order to reduce leakage of the precursor polymer mixture as it is cured under applied compression, sealant was applied between the sliding sample mold and the copper bar. A flat "pad" is formed by squeezing the uncured mixture between the upper and lower bars during curing (Figure 4.1b). The samples were cured by setting the copper bars to 50 °C and maintaining this temperature and the desired applied load for 3

hours. Curing temperature of 50 °C was selected to balance competing effects between curing time and resultant mechanical/thermal properties (see Appendix C, Figure C3). The applied load during this curing process was set as a process variable and ranged from 0 to 4.5 MPa. It is important to note that the pressure during curing is denoted as the "curing pressure," and this value is reported as the initial applied pressure during curing (*i.e.*, a small amount of pressure relaxation is observed during the curing process). Additionally, note that the curing pressure is distinct from the applied pressure during thermal conductivity measurements, which is denoted as the "measurement pressure." Unless other stated, the measurement pressure in this work is ~ 0.2 to 0.3 MPa during thermal conductivity measurements. Importantly, this work reveals that the thermal conductivity of cured composites is insensitive to measurement pressure (discussed in detail in Section 4.5). This means that thermal conductivity enhancements that arise from applied curing pressure are preserved even if the mechanical load is removed after curing.

The final thickness of the cured composites depends on the curing pressures (0 to 4.5 MPa), with larger curing pressures leading to thinner samples. To ensure that sample thickness did not affect the data interpretation, I designed additional experiments with the 100 cSt samples where the final thickness was kept constant. This was done by scaling the volume of the uncured/uncompressed sample in such a way that the final thickness of the cured composite resulted in a thickness of ~ 1.5 mm. The following sections discuss the thermal properties and microscopy morphology of the resulting composite pads with LM fillers as well as pads with combined LM and Ag co-fillers.

4.3 Thermal Characteristics of V-PDMS Composite Pads

4.3.1 LM Fillers only

The thermal impact of precursor polymer solution pre-cure viscosity (~100 cSt vs. ~2,300 cSt) and curing pressure (no pressure vs. ~0.4 MPa) was first characterized on LM-only composite pads. It was found that the pre-cure viscosity does not impact the thermal conductivity of the pads made with only polymer matrix itself (both are 0.4 W m^{-1} K^{-1}) or of the LM-only composite pads cured without a mechanical load. Specifically, the 1.24 W m^{-1} K^{-1} for the 2,300 cSt matrix and the 1.3 W m^{-1} K^{-1} for the 100 cSt matrix (see Figure 4.2a) are comparable with the rather ordinary prior results on LM-only composite pads (typically in the 1 to 2 W m^{-1} K^{-1} range for 50% LM volume fraction[26,36,52,102]).

Curiously, applying ~0.4 MPa compressive pressure during curing of the LM-only composite pads only increases the thermal conductivity of the 100 cSt matrix composite. As illustrated in Figure 4.2a, when cured under load, the conductivity increases ~20% to 1.6 W m^{-1} K^{-1} for the lower viscosity matrix but is equal to 1.26 W m^{-1} K^{-1} for the 2,300 cSt matrix (*i.e.*, effectively equivalent to that without load).

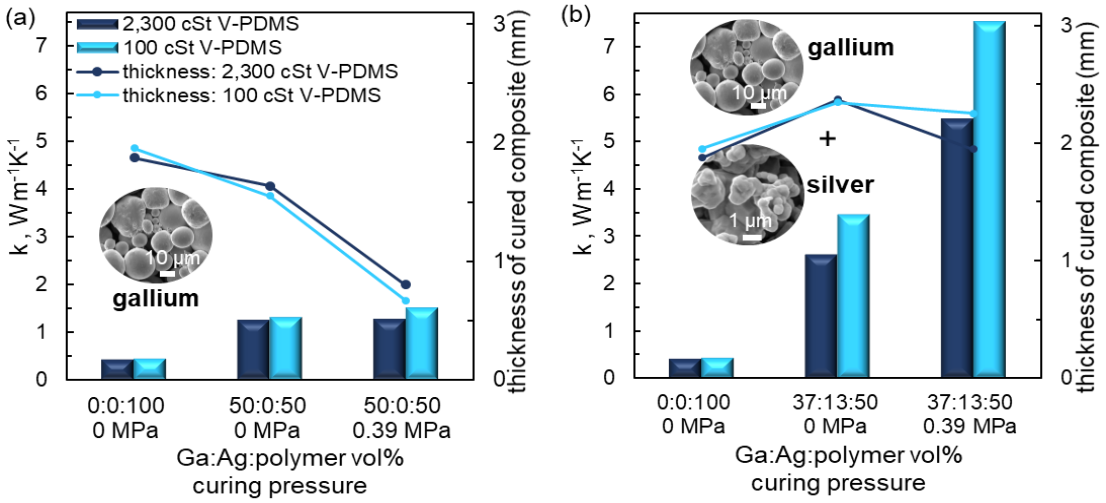

Figure 4.2: Impact of the pre-cure polymer matrix viscosity (100 cSt and 2,300 cSt) and compressive pressure during curing (no pressure vs. 0.4 MPa) on the thermal conductivity of the **(a)** LM-only composite pads and the **(b)** LM and Ag composite pads. Each data point represents the average value of three repetitions.

The electron micrographs of the composite pad cross-sections as shown in Figure 4.3) illustrate the underlying mechanisms of response to curing pressure and matrix pre-cure viscosity. Decoupling the matrix viscosity, *i.e.*, regardless of the matrix pre-cure viscosity, LM-only composite pads cured without a load consist primarily of separate and nearly spherical liquid microdroplets (see Figure 4.3a and Figure 4.3c).

As the curing pressure is applied, the LM fillers embedded in the compressed higher viscosity matrix (2,300 cSt) elongate in the direction perpendicular to the load applied during curing (see Figure 4.3b). This feature is preserved by the curing process and implies that the 2,300 cSt viscosity precursor polymer solution does not easily displace from in-between the fillers. The non-displaced precursor polymer matrix solution and unruptured oxide shells keep the encapsulated droplets isolated from the neighboring droplets. This microstructural feature of the higher viscosity sample prevents

the formation of thermal percolation paths with interconnected features and thus yields a lower thermal conductivity.

As the pre-cursor viscosity is lowered to 100 cSt, the cross-sectional micrograph of the 100 cSt LM-only composite pad cured under load reveals many interconnected droplets (see Figure 4.3d), which contrasts with what was observed in the 2,300 cSt viscosity precursor polymer pad. This observation confirms that within the 100 cSt matrix, the applied load displaces the precursor polymer solution between fillers, ruptures the Ga oxide shell on the LM droplets, and produces a higher degree of connectivity between the fillers.

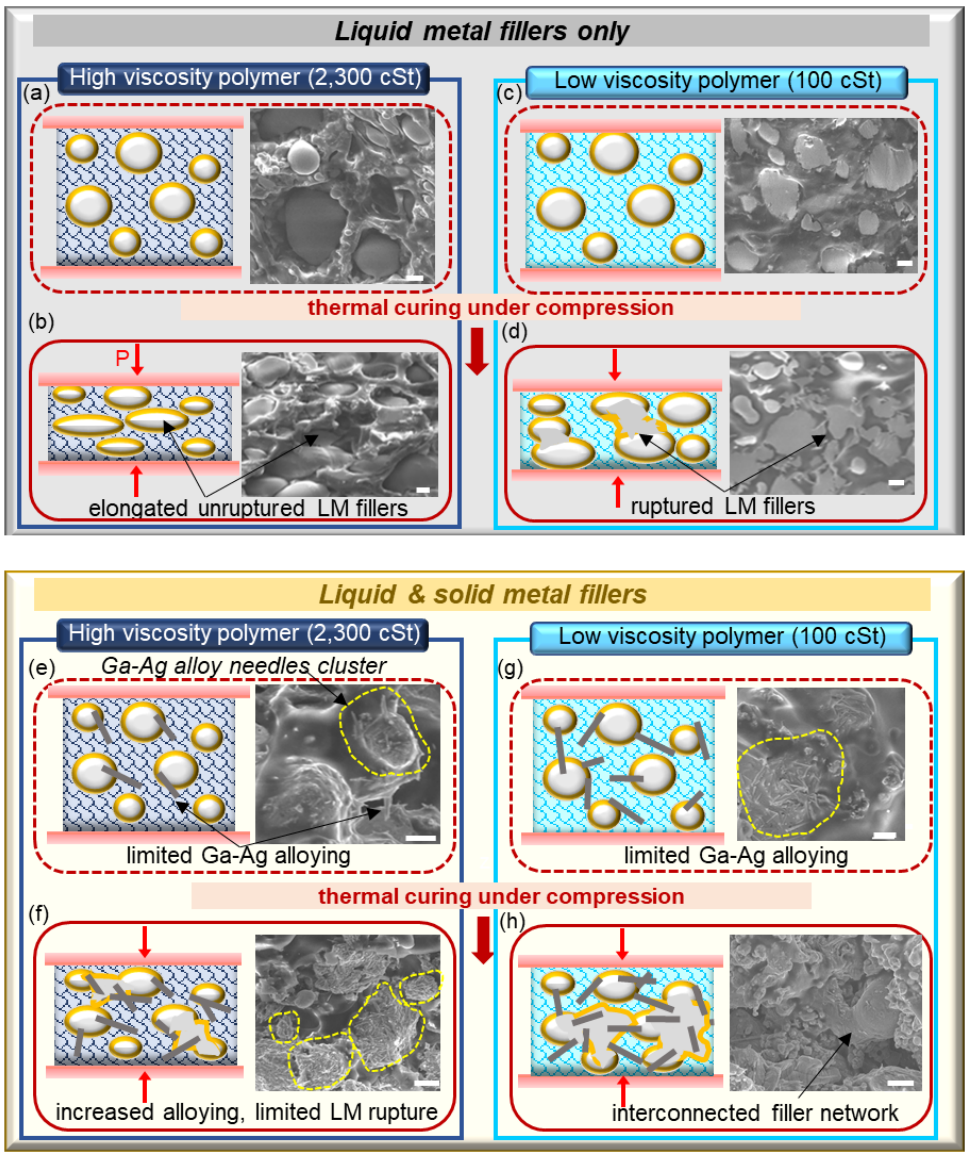

Figure 4.3: Microscale morphology of the (a-d) LM-only and (e-h) LM and Ag composites for different pre-cure polymer matrix viscosity (low = 100 cSt and high = 2,300 cSt) and compressive pressure during curing (no imposed pressure vs. 0.4 MPa). The scale bars correspond to 10 µm. The dotted yellow outlines in the images highlight regions where the needle-like Ga-Ag alloys are visible (additional images of the nanoneedles at higher magnification are available in the Appendix C, Figure C4)

However, this approach of using curing pressure to overcome interfacial thermal resistance between fillers and matrix for LM-only composites is limited by the overall fluidity of the LM-polymer mixture. Specifically, despite the tightly applied sample

mold, the LM-polymer mixture leaks even under the mild 0.4 MPa pressure, which results in thin pads (0.7 mm for 100 cSt and 0.8 mm for 2,300 cSt samples, see Figure 4.2a). Further increasing the pressure, results in leakage of the majority of the sample with only a small amount of residual sample left on the bars (*i.e.*, a suitable pad is not formed). The following section discusses how adding solid reactive particles resolves this issue.

4.3.2 Ag and LM Co-Fillers

Similar to the LM-fillers-only composite pads, thermal impact of the precursor polymer solution pre-cure viscosity (~100 cSt vs. ~2,300 cSt) as well as the curing pressure (no pressure vs. 0.4 MPa) on composite pads with both Ag and LM co-fillers is evaluated. First, considering samples cured without load, the thermal conductivity enhancement in these multi-phase filler composite pads relative to LM-only composites is evident from the data in Figure 4.3b. These pads measured thermal conductivities of 2.6 and 3.5 W m^{-1} K^{-1} for the 2,300 and 100 cSt matrices, respectively (versus 1.24 and 1.3 W m^{-1} K^{-1} for the LM-only composite pads described in Section 4.3.1). As explained in the previous sections, some alloying between the Ag and LM fillers occurs even during mixing prior to sample casting. The higher thermal conductivity of the 100 cSt matrix sample stems from the lower pre-cure viscosity solution promoting a higher degree of contact and alloying of fillers during mixing than the 2,300 cSt matrix (evidenced by the amount of visible alloy nanoneedle formation observed in the electron micrographs of Figure 4.3e and g).

In addition to the matrix pre-cure viscosity, the impact of curing pressure as a parameter on the thermal conductivity and thickness of the multi-phase filler composite pads is also evaluated. The combined benefits of applied curing pressure, lower pre-cure viscosity, and combined LM and Ag co-fillers are evident through the thermal conductivity and thickness data in Figure 4.2b. Applying 0.4 MPa of curing pressure approximately doubles the composite pad thermal conductivity relative to no applied pressure. In addition, the lower pre-cure matrix viscosity promotes increased Ag-Ga alloy formation and reaches a value of 7.6 W m^{-1} K^{-1}. Notably, the addition of the solid Ag particles inhibits leakage of the polymer precursor mixture during curing and addresses the issue described with the LM-filler-only pads cured under pressure in the previous section. The thickness of cured composites with and without applied curing pressure is similar to Figure 4.2b, whereas a large drop in thickness is seen in the LM-fillers-only cured composites in Figure 4.2a.

The cross-sectional electron micrographs in Figure 4.3e-h illustrate a high degree of LM droplet "smudging" and nanoneedle formation in all of the samples. Thus, as expected, the alloying process increases the fillers' interconnectivity and enhances the composite's thermal conductivity. The thermal data indicates that the process is promoted by lowering the pre-cure viscosity of the polymer matrix and applying the compressive load during the thermal curing process. In simple terms, both of these factors allow more direct contact between solid and liquid particles, while the applied load also facilities the rupture of the oxide shell. The application of curing pressure is critical because only limited alloying occurs when Ag is gently mixed with Ga (evident from cross-sectional

electron micrographs in Figure 4.3e and g). The magnitude of the curing pressure impacts these microscopic mechanisms, and in the next section the curing pressure parameter is systematically explored.

4.4 Impact of Curing Pressure on Composites

4.4.1 V-PDMS Composites with Ag and LM Co-Fillers

The data in the previous sections reveals that curing pressure is one of the critical parameters that enhance the thermal transport in composite pads. In this section, curing pressure is investigated in detail to understand its implications on the functional properties of the pads. Figure 4.4 illustrates the effect of varying curing pressure on the thermal conductivity and thickness of low and high pre-cure matrix viscosity samples with solid and liquid co-fillers. In agreement with the above results, thermal conductivity increases as curing pressure increases and/or pre-cure viscosity decreases. For samples with the 100 cSt precursor polymer formation, this increase is approximately linear up to ~2 MPa and reaches a thermal conductivity of ~15 W m^{-1} K^{-1}. The thermal conductivity of the lower viscosity matrix samples is less sensitive to curing pressures in the ~2 MPa to 4.5 MPa range and spans the 15 to 20 W m^{-1} K^{-1} range. The 100 cSt precursor polymer solution composites have a noticeably higher thermal conductivity than the 2,300 cSt samples throughout the entire curing pressure range.

Increasing the curing pressure ruptures the LM fillers and forms thermally conductive bridges within the low viscosity polymer matrix as shown in the cross-sectional electron micrograph in Figure 4.4c. This increased connectivity within the

matrix enhances the thermal conductivity of the composite as the curing pressure is increased. The presence of unruptured LM fillers in the higher viscosity polymer pads shows a decrease in filler connectivity relative to the lower viscosity polymer pads (Figure 4.4c-d). Upon increasing the curing pressure, enhanced alloying is observed between the LM and Ag fillers, but the presence of unruptured LM fillers explains the smaller increase in the thermal conductivity for the samples that used the precursor solution with higher viscosity.

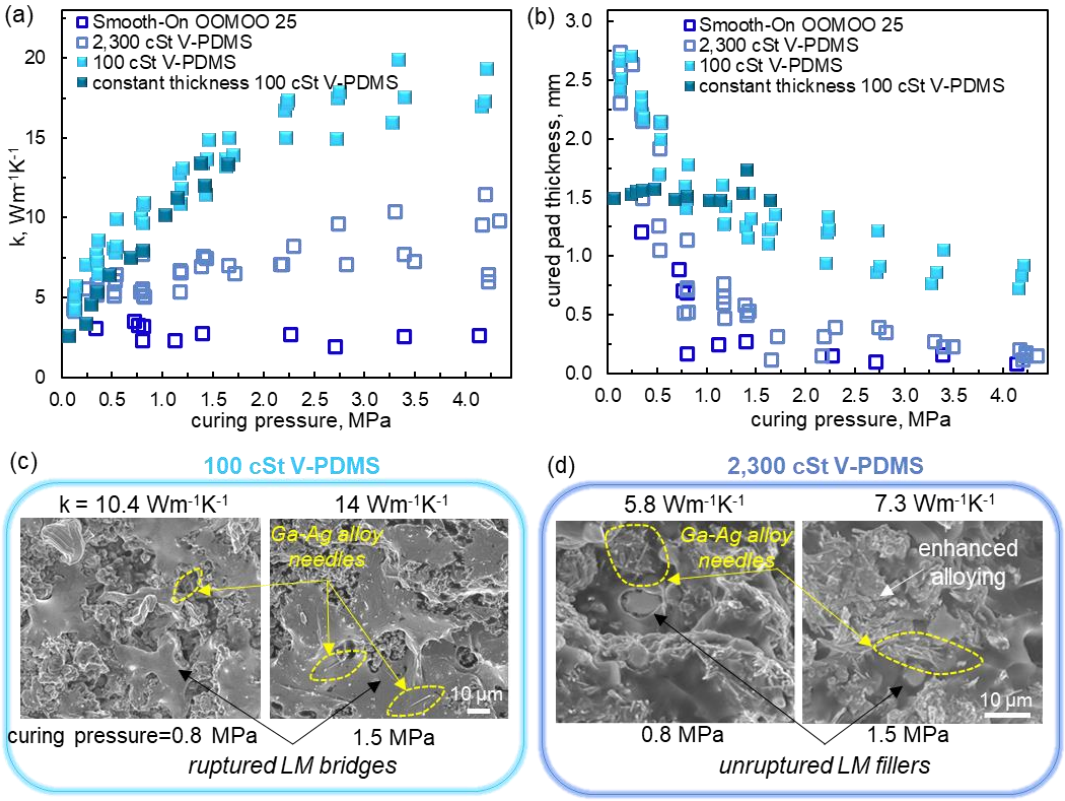

Figure 4.4: (a) The thermal conductivity and (b) corresponding thickness of 100 cSt V-PDMS, 2,300 cSt V-PDMS, and Smooth-on OOMOO-25 (~3,500 cSt pre-cure viscosity) composite pads with LM and Ag co-fillers as function of curing pressure. Each data point represents a different sample. Illustrative electron micrographs of (c) 100 cSt V-PDMS and (d) 2,300 cSt V-PDMS composite pads cured under 0.8 MPa and 1.5 MPa compression.

4.4.2 Commercial Polymer Kits Composites with Ag and LM Co-Fillers

Additional experiments were performed with a commercial "off-the-shelf" two-part silicone polymer kit that researchers commonly employ. The commercial polymer kits have viscosities on the order of several thousand cSt, and so these were expected to behave similar to the 2,300 cSt V-PDMS samples, but this was not the case. Samples were fabricated with the commercially available Smooth-on OOMOO-25 kit. It was found that the thickness of the OOMOO-25 samples trended similarly with curing pressure to the 2,300 cSt V-PDMS data (see Figure 4.4b), however, the thermal conductivity data trended quite differently (see Figure 4.4a). The thermal conductivity of the OOMOO-25 samples was consistently lower than the 2,300 cSt V-PDMS data and was insensitive to curing pressure. One possible reason for this thermal conductivity difference could be the presence of silica particles in the polymer solution that the manufacturer originally put in place (see Appendix C, Figure C5). The presence of these silica particles could disrupt the formation of a metallic percolation network. In addition, the pot life of the OOMOO-25 kit is only 15 min and this short amount of processing time could affect the ability to rupture the LM oxide shell and achieve good filler-filler contact. The collective results in this section indicate that the polymer matrix for the composite fabrication must be carefully selected.

4.4.3 Decoupling Role of Pressure and Thickness on Thermal Transport

It is evident from Figure 4.4b, that as the curing pressure is increased, the cured sample thickness decreases. In order to ensure that the enhancement in the thermal conductivity *i.e.,* drop in the thermal resistance is due to the enhancement in thermal

transport due to the curing pressure and not due to the decrease in the thickness, additional experiments were performed. More specifically, the thermal conductivity measured in this work is an effective property that includes the thermal resistance of the sample itself as well as the thermal contact resistance between the sample and the SBA bars. The thinnest 100 cSt V-PDMS samples were ~ 1 mm thick, and this is much larger than the sub-10 μm particle sizes for the LM and Ag filler particles. Consequently, the true thermal conductivity of the sample should not be affected by sample thickness. To confirm that sample thickness is not affecting the data interpretation, a set of samples that had a final constant thickness of ~1.5 mm regardless of the applied curing pressure were fabricated. The measured thermal conductivity of these constant thickness samples overlaps with the variable thickness samples (labeled "constant thickness 100 cSt V-PDMS" in Figure 4.4a), and this indicates that thermal contact resistance does not play an important role in the measurements (or that this effect is at least smaller than the thermal conductivity uncertainty resulting from sample-to-sample variations). The next section discusses the impact of thermal contact resistance in detail.

4.5 Role of Thermal Contact Resistance on Thermal Conductivity of Cured Polymer Pads

In addition to confirming equivalent thermal conductivities for samples with variable thickness and constant thickness in the above section, two additional experiments were conducted to ensure the thermal contact resistance had a minimal effect on the measured functional properties of the composite pads. First, it was confirmed that

the measured thermal conductivity is not a function of applied measurement pressure. Second, the possibility of artificially-low thermal contact resistances was investigated that could result from curing samples directly within the thermal conductivity measurement system.

Figure 4.5 shows that the thermal conductivity of the polymer composite pads (37:13:50 Ga:Ag:V-PDMS$_{100\ cSt}$ v/v) prepared with the low viscosity precursor polymer solution does not depend on measurement pressure. This insensitivity to measurement pressure is confirmed for three different curing pressure of 0 MPa, 0.8 MPa, and 1.5 MPa. Thermal contact resistance is typically a measure of pressure and this insensitivity to measurement pressure indicates that either the thermal contact resistance in this particular study is insensitive to measurement pressure or that the thermal contact resistance itself is small. The approximately constant thermal conductivity for each curing pressure indicates that it is the curing pressure that determines the thermal conductivity of the sample, and that the thermal conductivity is compression-activated. Importantly, the high thermal conductivities achieved through compression-activation remain in place even if the curing pressure is removed and the polymer pad can be used in low-load applications post-cure.

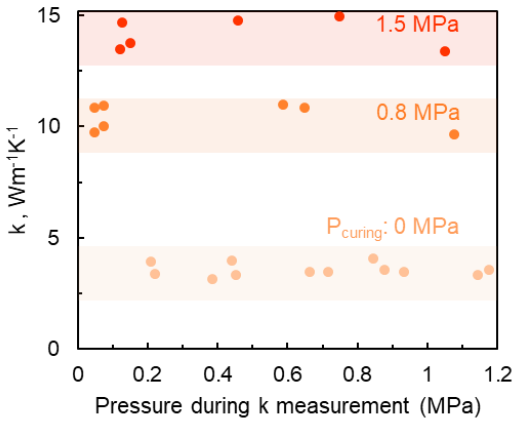

Figure 4.5: Thermal conductivity of cured pads (37:13:50 v/v Ga:Ag:V-PDMS$_{100\ cSt}$) as measurement pressure varies. The measurement pressure was varied by removing the curing pressure from the sample once it was cured. Sample was not removed from the bar and measurement pressure was varied for the above measurements.

Additional experiments were performed to investigate the possibility of artificial suppression of thermal contact resistance by directly curing the samples on the SBA bars in the thermal conductivity measurement system. The amount of physical contact at an interface between two materials can often be significantly less than 100% due to micro-roughness, and this is a primary driver for thermal contact. By directly curing the polymer composites in the SBA bars, the physical contact between the polymer composite and the SBA bar is exceptionally good (*i.e.*, the liquid state of the uncured polymer composite allows them to conform extremely well to the micro roughness of the SBA bars). In this set of experiments, two thermal conductivity measurements for each sample were performed. First, the thermal conductivity was measured by leaving the samples on the SBA bars after curing and then proceeding to thermal conductivity measurements at the desired measurement pressure. After this first measurement, the samples were physically removed from the SBA bars and then placed back on the SBA bars. This physical removal and reapplication disrupts the alignment of the polymer pad

with microroughness on the SBA bar and should lead to an increase in thermal contact resistance (and hence a decrease in measured thermal conductivity). This experiment was done for three different curing pressures, and in all cases the thermal conductivity is very similar both without and with removal from the SBA bars (see Appendix C, Figure C6). This result indicates that this effect does not have a meaningful impact on the overall interpretation of the results presented in this work and hence demonstrates that any potential suppression of thermal contact resistance by directly curing on the SBA bars is very small.

4.6 Mechanical Characteristics and Morphology of LM-Ag Composite Pads

Along with the thermal properties of the composite pads, mechanical characteristics need to be balanced to ensure that the functional properties of the pads enable their use in various application areas. This section discusses the intercoupling between curing pressure, viscosity of the precursor polymer solution, and composite mechanical characteristics. It is observed that the lower viscosity polymer composite pads were less compliant and more brittle than the higher viscosity polymer composite pads throughout the entire curing pressure range of 0 – 4.5 MPa (see Figure 4.6).

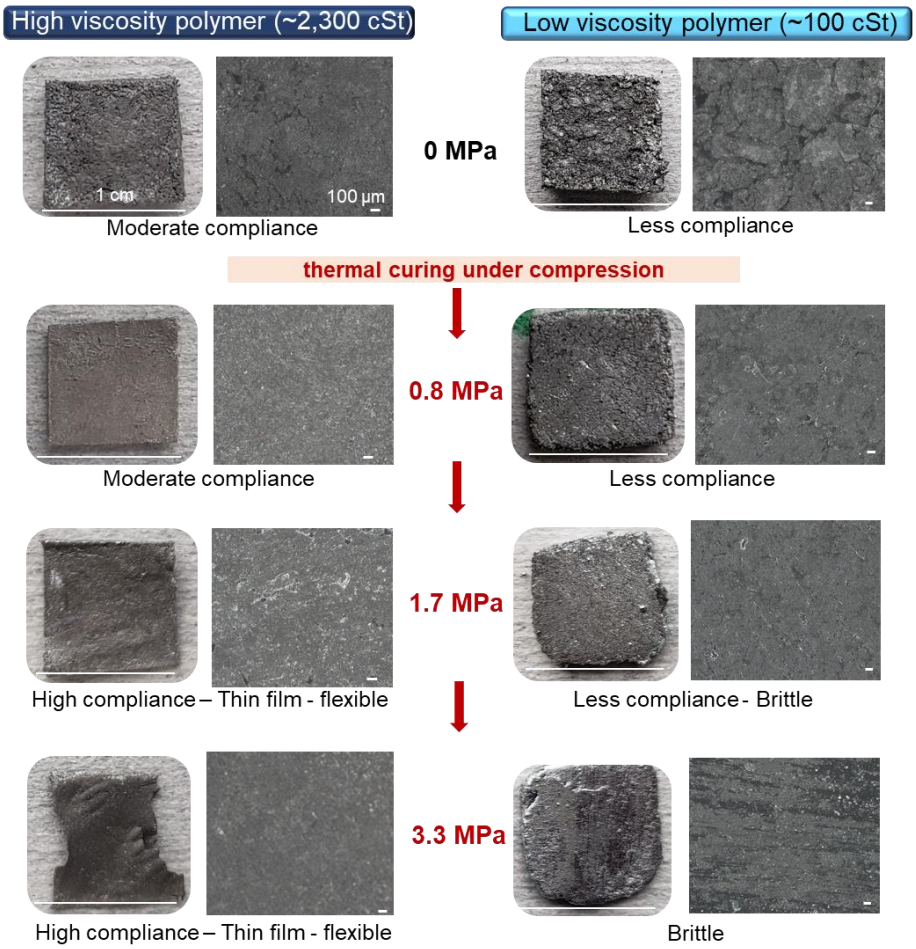

Figure 4.6: Impact of matrix viscosity, pressure during curing, and thickness on mechanical characteristics and macroscopic composition

This decreased compliance is attributed to two main effects. First, the lower viscosity polymer composite pads exhibit more alloying between the Ag and Ga fillers and this process should stiffen the composite. Second, at higher curing pressures (*e.g.*, $\gtrsim$ 1.7 MPa for the precursor polymer solution with lower viscosity), the composite began to noticeably leak outside of the sample mold. Since the Ag and Ga fillers have solidified into a stiff alloy network, it is suspected that this leakage is primarily uncured precursor polymer solution and that the 50 vol% fraction of polymer matrix is no longer maintained

at these elevated curing pressures (*i.e.*, a decrease in soft polymer content leads to a more brittle composite). In contrast to the lower viscosity polymer pads, the higher viscosity polymer pads maintained mechanical compliance throughout the entire range of curing pressures. This maintained compliance is believed to originate from the absence of a stiff alloy network formation between the Ag and Ga fillers. In addition, at higher curing pressures when leakage began to noticeably occur (*e.g.*, $\gtrsim$ 0.8 MPa for the precursor polymer solution with higher viscosity), that leakage was likely not selective and consisted of precursor polymer solution, Ag filler, and Ga filler. This means that the 50 vol% fraction of polymer matrix in these composites would be roughly maintained and so would the corresponding mechanical compliance. It was also observed that when applying curing pressure, the lower viscosity polymer composite pad is thicker than the higher viscosity polymer composite pad as discussed in the previous sections. This is attributed to the presence of the stiff Ag-Ga network in the samples that used the precursor polymer solution with lower viscosity, which likely inhibits sample leakage while curing under compression. The qualitative observations in this section highlight that increasing curing pressure beyond a certain point has diminishing benefits and that further research will be necessary to balance the materials composition, thermal properties, mechanical properties, and curing pressure of these solid-phase polymer TIMs, which is discussed in detail in the last chapter as future work.

4.7 Conclusion

In this chapter, I have introduced a multifaceted strategy to enhance the thermal conductivity of cured polymer composites. This strategy synergistically combines three key characteristics: reactive solid and liquid fillers, a polymer matrix with low pre-cure viscosity, and mechanical compression during thermal curing. Each of these characteristics play a key role in creating the high thermal conductivity polymer composite. The low pre-cure matrix viscosity and mechanical compression during thermal curing facilitates direct physical contact between the composite's co-filler materials (Ga LM droplets and solid Ag particles) and rupture of the oxide shell on droplet surface. Upon physical contact, the Ga and Ag react to form needle-like intermetallic alloy structures. These needle-like alloys in turn promote the formation of a percolated network of Ga, Ag, and Ag-Ga alloy. The end result of this multifaceted strategy is the achievement of a solid-phase polymer TIM pad with a high thermal conductivity of ~ 15 W m^{-1} K^{-1} (for a curing pressure of 2 MPa). Importantly, this high thermal conductivity is maintained even after the removal of the curing pressure, which means that these pads can be used in typical low-pressure TIM applications (0.2 - 0.3 MPa, *i.e.*, less than 50 psi). One of the key discoveries in this chapter is that pre-cure viscosity of the polymer matrix should be significantly smaller than that of typical two-part polymer kits (on the order of 10^2 cSt versus 10^3 cSt). This finding will have important implications for developing next-generation solid-phase polymer TIMs.

CHAPTER 5

5. CONCLUSION AND FUTURE DIRECTIONS

5.1 Dissertation Summary

In the pursuit of advancing the performance of TIMs, this work presents the integration of LM in polymers to develop composites with tunable functional properties. My research employs a holistic approach to comprehensively design LM-based TIMs by addressing some of the underlying fundamental challenges at each stage- starting from the use of LM as fillers to their integration in a polymer matrix, hence utilizing the LMs to their full potential as TIM materials. Throughout this work, I have focused on unraveling the mechanisms and processes governing the thermal transport within a soft composite which has led to the development of thermally enhanced LM-based grease and gap pad. The key fundamentals investigated in this work will serve as guidelines for tuning polymer composites' thermal and mechanical characteristics.

LM as filler material was investigated which led to addressing the fundamental knowledge gap of how the LM thin native oxide shells influence the thermal transport in LMs. Here, I studied the rupture mechanics of LM capsules which revealed the important parameters governing the interfacial interaction of LM. Effective bridging of LM fillers will occur once the oxide shell “pops” which will lead to the formation of numerous thermal percolation pathways. LM capsule age, diameter, and oxide shell manipulation via chemical treatment are identified as critical parameters that have implications on the functional properties of LM as fillers. This led to identifying the desired LM attributes

which would result in better heat dissipation under pressures that are relevant for TIM applications.

Following the identification of optimal LM filler characteristics, integration in an uncured polymer matrix introduces additional thermal resistances. I demonstrated the role of polymer viscosity in forming thermal network between the LM fillers. The matrix acts as an additional physical barrier in-between the fillers and reducing the matrix viscosity can help facilitate filler contact during compression. Here, it is also highlighted that tuning the matrix viscosity is not sufficient to achieve ample bridging of LM fillers. The introduction of reactive solid Ag metal co-fillers facilitates popping of LM oxide since they act as activation sites and serve as thermal anchors that connect the LM fillers in the matrix. Reactive co-fillers in conjunction with pressure and matrix viscosity tuning are required to induce the oxide shell "popping" to achieve thermal percolation, and hence thermally enhanced greases can be developed. Compositional tuning of the hybrid fillers and filler processing techniques such as premixing fillers to form continuous filler network can also lead to thermal enhancement but degrade the other functional properties such as compressibility. Striking a balance between the thermal and mechanical properties is critical, and this work presents the key design parameters that can be tuned to achieve the desired functional properties.

In the final section, the key focus is to ensure that the thermally enhanced features obtained by tuning each of the components *i.e.*, fillers, and matrix are preserved when the composite is cured. One of the key findings here is that pre-cure viscosity of the polymer matrix should be significantly smaller than that of typical two-part polymer kits (on the

order of 10^2 cSt versus 10^3 cSt). This finding will have important implications on the development of next-generation solid-phase polymer TIMs. Further, the importance of employing external stimuli as an activation mechanism during the composite curing stage is key to preserving the thermal percolation pathways and reducing interfacial resistances.

As mentioned previously, this work is anchored on three research cores: 1) interfacial interaction of LM fillers, 2) polymer rheology-dependent thermal network, and 3) external stimuli-activated thermal pathways. These core areas are investigated throughout my research. Overall, this work presents a multifaceted strategy to enhance the functional properties of polymer composites by offering new insights on the LMs interfacial interactions between LM fillers and reactive metallic co-fillers, matrix rheology pre-curing and in-situ activation mechanisms provide the basis for further study in the development of thermally enhanced composites. The mechanisms identified in this work contribute towards the fundamental knowledge about LM filler interaction with LM fillers, polymers and other reactive metal fillers, which sets the foundation for preparing LM-based composites with tunable functional properties.

5.2 Future Directions

This work can be extended in a few directions with a focus on enhancing the mechanical properties of the LM-based polymer composites. One of the ways this can be done is by tuning the polymer formulation of individual components such as the molar ratio of crosslinker to chain extender and to the polymer base of the custom V-PDMS. The research in this work was limited to using a fixed ratio of the different constituents of

V-PDMS, which allowed to keep the viscosity of matrix in the identified thermally beneficial regime. Modulating the individual constituents' ratios while keeping the same low viscosity and filler ratio will provide better control on the mechanical compliance of the composites.

This research has explored only one reactive metal co-filler *i.e.,* Ag with Ga LM. The use of solid metal fillers that react and alloy with LM do provide challenges due to the increase in the rigidity of the composites, but this work shows that compositional tuning can help to find the balance between the thermal and mechanical properties. This use of solid metal additives can be explored as a way to help mitigate the risk of LM composites reacting with neighboring components. Focusing on the precise control of unreacted LM, can also help in improving the reliability concerns of these composites. With the introduction of non-reactive solid fillers with LM fillers or using non-reactive metals with engineering-coated surfaces to allow for more compliance, the parameters of curing force, and filler composition tuning required to achieve thermal percolation will need to be investigated in detail. Further, I expect the thermal bridging mechanism and functional properties will also change with the type of filler used (filler size and shape *i.e.,* 0D, 2D, or 3D), for example, if graphene or carbon nanotubes are used as co-fillers with LM, the interactions between them will be significantly different than the Ga-Ag interactions where rapid alloying occurs. The introduction of co-fillers to enhance other functional properties such as EMI shielding can further be explored. The chemically-altered LM fillers that showed better thermal transport in the absence of polymer, can be

integrated in the polymer matrix to develop greases and gap pads that can require a lower curing pressure for activation.

Some additional filler networking strategies can be explored to enhance and control the in-plane and through-plane orientation of fillers. This work highlights the use of pressure pre-curing the composite. This technique of employing external stimuli before curing can be extended to combing strategies like a magnetic field or electric field induced orientation of fillers pre-curing and then using sintering process to develop cured composites.

Another exploration this work can drive is the development of smart, self-healing TIMs. Similar to the use of LM in self-healing electrical conductors, the presence of additional sacrificial LM fillers which can be ruptured and released to heal the composites and restore thermal network can be explored. With the integration of reactive metal co-fillers, the increase in mechanical rigidity along with enhancement in thermal properties with compression-induced percolation, this work can be expanded to other thermal management strategies such as development of LM composite heat spreaders. Overall, the mechanisms identified in this work and strategies adopted to develop LM-based composites have strong potential in different applications such as thermal management, electronic interconnects, soft electronics, and additive manufacturing.

REFERENCES

1. Black, B. *et al.* Die stacking (3D) microarchitecture. in *Proceedings of the 39th Annual IEEE/ACM International Symposium on Microarchitecture* 469–479 (IEEE Computer Society, 2006).

2. Beyne, E. The rise of the 3rd dimension for system integration. in *2006 International Interconnect Technology Conference* 1–5 (IEEE, 2006).

3. Chiu, C.-P., Chang, J.-Y. & Saha, S. Thermal management of packages with 3D die stacking. in *2012 7th International Microsystems, Packaging, Assembly and Circuits Technology Conference (IMPACT)* 201–204 (IEEE, 2012).

4. Moore, A. L. & Shi, L. Emerging challenges and materials for thermal management of electronics. *Mater. today* **17**, 163–174 (2014).

5. Bar-Cohen, A. & Wang, P. Thermal Management of On-Chip Hot Spot. *J. Heat Transfer* **134**, 553–567 (2012).

6. Razeeb, K. M., Dalton, E., Cross, G. L. W. & Robinson, A. J. Present and future thermal interface materials for electronic devices. *Int. Mater. Rev.* **63**, 1–21 (2018).

7. Wang, J. *et al.* Impact of Nanoscale Roughness on Heat Transport across the Solid–Solid Interface. *Adv. Mater. Interfaces* **7**, 1901582 (2020).

8. Prasher, R. Thermal interface materials: historical perspective, status, and future directions. *Proc. IEEE* **94**, 1571–1586 (2006).

9. Zhang, Y., Ma, J., Wei, N., Yang, J. & Pei, Q.-X. Recent progress in the development of thermal interface materials: a review. *Phys. Chem. Chem. Phys.* **23**, 753–776 (2021).

10. Zhou, Y. *et al.* Recent advances in thermal interface materials. *ES Mater. Manuf.* **7**, 4–24 (2020).

11. Shahil, K. M. F. & Balandin, A. A. Thermal properties of graphene and multilayer graphene: Applications in thermal interface materials. *Solid State Commun.* **152**, 1331–1340 (2012).

12. Sarvar, F., Whalley, D. C. & Conway, P. P. Thermal interface materials-A review of the state of the art. in *2006 1st electronic system integration technology conference* vol. 2 1292–1302 (IEEE, 2006).

13. Prasher, R. S., Shipley, J., Prstic, S., Koning, P. & Wang, J. Thermal Resistance of

Particle Laden Polymeric Thermal Interface Materials. *J. Heat Transfer* **125**, 1170 (2003).

14. Saborio, M. G. *et al.* Liquid Metal Droplet and Graphene Co-Fillers for Electrically Conductive Flexible Composites. *Small* **16**, 1903753 (2020).

15. Sun, Y. & Shi, G. Graphene/polymer composites for energy applications. *J. Polym. Sci. Part B Polym. Phys.* **51**, 231–253 (2013).

16. Das, T. K. & Prusty, S. Graphene-based polymer composites and their applications. *Polym. Plast. Technol. Eng.* **52**, 319–331 (2013).

17. Chou, H.-E., Yang, S.-R., Wang, S.-F. & Sung, J. C. Thermal Conductivity of Diamond-Containing Grease. *J. Electron. Packag.* **132**, 041015 (2010).

18. Ma, H. *et al.* Strategies for enhancing thermal conductivity of polymer-based thermal interface materials: A review. *J. Mater. Sci.* **56**, 1064–1086 (2021).

19. Mehra, N., Mu, L., Ji, T. & Zhu, J. Chapter 3 - Thermal Conduction in Polymer Composites. in (eds. Song, K., Liu, C. & Guo, J. Z. B. T.-P.-B. M. N. and T. A.) 77–110 (Elsevier, 2019). doi:https://doi.org/10.1016/B978-0-12-815067-2.00003-2.

20. Chou, H.-E., Yang, S.-R., Wang, S.-F. & Sung, J. C. Thermal conductivity of diamond-containing grease. *J. Electron. Packag.* **132**, (2010).

21. Ren, J. *et al.* Enhanced thermal conductivity of epoxy composites by introducing graphene@ boron nitride nanosheets hybrid nanoparticles. *Mater. Des.* **191**, 108663 (2020).

22. Seyed Esfahani, S. A., Ghahramani, N., Mehranpour, M. & Nazockdast, H. Rheological, thermal, and electrical characterization polyamide/polypropylene blend composites containing hybrid filler: Boron nitride and reduced graphene oxide. *SPE Polym.* **2(2)**, pp.134-144 (2021).

23. Teng, C.-C., Ma, C.-C. M., Chiou, K.-C., Lee, T.-M. & Shih, Y.-F. Synergetic effect of hybrid boron nitride and multi-walled carbon nanotubes on the thermal conductivity of epoxy composites. *Mater. Chem. Phys.* **126**, 722–728 (2011).

24. Fu, Y.-X., He, Z.-X., Mo, D.-C. & Lu, S.-S. Thermal conductivity enhancement with different fillers for epoxy resin adhesives. *Appl. Therm. Eng.* **66**, 493–498 (2014).

25. Chen, Y. *et al.* Constructing a “pea-pod-like” alumina-graphene binary

architecture for enhancing thermal conductivity of epoxy composite. *Chem. Eng. J.* **381**, 122690 (2020).

26. Ralphs, M. I. *et al.* In Situ Alloying of Thermally Conductive Polymer Composites by Combining Liquid and Solid Metal Microadditives. *ACS Appl. Mater. Interfaces* **10**, 2083–2092 (2018).

27. Prasher, R. S., Koning, P., Shipley, J. & Devpura, A. Dependence of Thermal Conductivity and Mechanical Rigidity of Particle-Laden Polymeric Thermal Interface Material on Particle Volume Fraction. *J. Electron. Packag.* **125**, 386 (2003).

28. Subramanian, V. *et al.* Mechanical Characterization of Thermal Interface Materials and Its Challenges. *J. Electron. Packag.* **141**, 1 (2019).

29. Lee, Y. J. Thermo-mechanical properties of high performance thermal interface gap filler pads. in *2010 12th IEEE Intersociety Conference on Thermal and Thermomechanical Phenomena in Electronic Systems* 1–8 (IEEE, 2010).

30. Prasher, R. Thermal Interface Materials: Historical Perspective, Status, and Future Directions. *Proc. IEEE* **94**, 1571–1586 (2006).

31. Cui, Y., Li, M. & Hu, Y. Emerging interface materials for electronics thermal management: experiments, modeling, and new opportunities. *J. Mater. Chem. C* **8**, 10568–10586 (2020).

32. Devpura Ravi S. Prasher, Amit, P. E. P. Size effects on the thermal conductivity of polymers laden with highly conductive filler particles. *Microscale Thermophys. Eng.* **5**, 177–189 (2001).

33. Wang, Q., Yu, Y. & Liu, J. Preparations, Characteristics and Applications of the Functional Liquid Metal Materials. *Adv. Eng. Mater.* **20**, 1700781 (2018).

34. Seshadri, I., Esquenazi, G. L., Cardinal, T., Borca-Tasciuc, T. & Ramanath, G. Microwave synthesis of branched silver nanowires and their use as fillers for high thermal conductivity polymer composites. *Nanotechnology* **27**, 175601 (2016).

35. Jia, L.-C. *et al.* Highly thermally conductive liquid metal-based composites with superior thermostability for thermal management. *J. Mater. Chem. C* **9**, 2904–2911 (2021).

36. Tutika, R., Zhou, S. H., Napolitano, R. E. & Bartlett, M. D. Mechanical and Functional Tradeoffs in Multiphase Liquid Metal, Solid Particle Soft Composites. *Adv. Funct. Mater.* 1804336 (2018) doi:10.1002/adfm.201804336.

37. Chung, S.-H., Kim, H. & Jeong, S. W. Improved thermal conductivity of carbon-based thermal interface materials by high-magnetic-field alignment. *Carbon N. Y.* **140**, 24–29 (2018).

38. Ralphs, M., Kong, W., Wang, R. Y. & Rykaczewski, K. Thermal Conductivity Enhancement of Soft Polymer Composites through Magnetically-Induced Percolation and Particle-Particle Contact Engineering. *Adv. Mater. Interfaces* **1801857**, 6 (2019).

39. Yun, G. *et al.* Liquid metal composites with anisotropic and unconventional piezoconductivity. *Matter* **3**, 824–841 (2020).

40. Xue, Y. *et al.* Improvement in thermal conductivity of through-plane aligned boron nitride/silicone rubber composites. *Mater. Des.* **165**, 107580 (2019).

41. Goto, T. *et al.* Movable cross-linked elastomer with aligned carbon nanotube/nanofiber as high thermally conductive tough flexible composite. *Compos. Sci. Technol.* **190**, 108009 (2020).

42. Guo, Y., Chen, Y., Wang, E. & Cakmak, M. Roll-to-Roll Continuous Manufacturing Multifunctional Nanocomposites by Electric-Field-Assisted "Z" Direction Alignment of Graphite Flakes in Poly(dimethylsiloxane). *ACS Appl. Mater. Interfaces* **9**, 919–929 (2017).

43. Thrasher, C., Farrell, Z., Morris, N., Willey, C. & Tabor, C. Mechanoresponsive Polymerized Liquid Metal Networks. *Adv. Mater.* **31(40)**, 1903864 (2019).

44. Silva, C. A. *et al.* Liquid Metal Based Island-Bridge Architectures for All Printed Stretchable Electrochemical Devices. *Adv. Funct. Mater.* **30**, 2002041 (2020).

45. Zhang, X. *et al.* Toward high efficiency thermally conductive and electrically insulating pathways through uniformly dispersed and highly oriented graphites close-packed with SiC. *Compos. Sci. Technol.* **150**, 217–226 (2017).

46. Hu, Y. *et al.* Vertically aligned carbon nanotubes grown on reduced graphene oxide as high-performance thermal interface materials. *J. Mater. Sci.* **55**, 9414–9424 (2020).

47. Daeneke, T. *et al.* Liquid metals: fundamentals and applications in chemistry. *Chem. Soc. Rev.* **47**, 4073–4111 (2018).

48. Yun, G. *et al.* Liquid metal-filled magnetorheological elastomer with positive piezoconductivity. *Nat. Commun.* **10**, 1–9 (2019).

49. Wang, J. *et al.* Printable superelastic conductors with extreme stretchability and robust cycling endurance enabled by liquid-metal particles. *Adv. Mater.* **30**, 1706157 (2018).

50. Tutika, R., Kmiec, S., Haque, A. B. M. T., Martin, S. W. & Bartlett, M. D. Liquid metal–elastomer soft composites with independently controllable and highly tunable droplet size and volume loading. *ACS Appl. Mater. Interfaces* **11**, 17873–17883 (2019).

51. Chen, S., Wang, H.-Z., Zhao, R.-Q., Rao, W. & Liu, J. Liquid metal composites. *Matter* **2**, 1446–1480 (2020).

52. Bartlett, M. D. *et al.* High thermal conductivity in soft elastomers with elongated liquid metal inclusions. *Proc. Natl. Acad. Sci.* **114**, 2143–2148 (2017).

53. Xu, Q., Oudalov, N., Guo, Q., Jaeger, H. M. & Brown, E. Effect of oxidation on the mechanical properties of liquid gallium and eutectic gallium-indium. *Phys. Fluids* **24**, (2012).

54. Tang, J. *et al.* Gallium-Based Liquid Metal Amalgams: Transitional-State Metallic Mixtures (TransM2ixes) with Enhanced and Tunable Electrical, Thermal, and Mechanical Properties. *ACS Appl. Mater. Interfaces* **9**, 35977–35987 (2017).

55. Hong, S. J. & Suryanarayana, C. Mechanism of low-temperature θ-Cu Ga 2 phase formation in Cu-Ga alloys by mechanical alloying. *J. Appl. Phys.* **96**, 6120–6126 (2004).

56. Kong, W. *et al.* High Thermal Conductivity in Multiphase Liquid Metal and Silicon Carbide Soft Composites. *Adv. Mater. Interfaces* 2100069 (2021).

57. Zhao, L., Chu, S., Chen, X. & Chu, G. Efficient heat conducting liquid metal/CNT pads with thermal interface materials. *Bull. Mater. Sci.* **42**, 192 (2019).

58. Sargolzaeiaval, Y. *et al.* High Thermal Conductivity Silicone Elastomer Doped with Graphene Nanoplatelets and Eutectic GaIn Liquid Metal Alloy. *ECS J. Solid State Sci. Technol.* **8**, P357–P362 (2019).

59. Mei, S., Gao, Y., Deng, Z. & Liu, J. Thermally conductive and highly electrically resistive grease through homogeneously dispersing liquid metal droplets inside methyl silicone oil. *J. Electron. Packag. Trans. ASME* **136**, 011009 (2014).

60. Yu, D. *et al.* A Super-Stretchable Liquid Metal Foamed Elastomer for Tunable Control of Electromagnetic Waves and Thermal Transport. *Adv. Sci.* **7**, 2000177

(2020).

61. Chiechi, R. C., Weiss, E. A., Dickey, M. D. & Whitesides, G. M. Eutectic gallium-indium (EGaIn): A moldable liquid metal for electrical characterization of self-assembled monolayers. *Angew. Chemie - Int. Ed.* **47**, 142–144 (2008).

62. Hohman, J. N. *et al.* Directing substrate morphology via self-assembly: Ligand-mediated scission of gallium-indium microspheres to the nanoscale. *Nano Lett.* **11**, 5104–5110 (2011).

63. Doudrick, K. *et al.* Different shades of oxide: From nanoscale wetting mechanisms to contact printing of gallium-based liquid metals. *Langmuir* **30**, 6867–6877 (2014).

64. Boley, J. W., White, E. L. & Kramer, R. K. Mechanically sintered gallium-indium nanoparticles. *Adv. Mater.* **27**, 2355–2360 (2015).

65. Lear, T. R. *et al.* Liquid metal particle popping: Macroscale to nanoscale. *Extrem. Mech. Lett.* **13**, 126–134 (2017).

66. Bartlett, M. D. *et al.* Stretchable, High-k Dielectric Elastomers through Liquid-Metal Inclusions. *Adv. Mater.* **28**, 3726–3731 (2016).

67. Finkenauer, L. R., Lu, Q., Hakem, I. F., Majidi, C. & Bockstaller, M. R. Analysis of the Efficiency of Surfactant-Mediated Stabilization Reactions of EGaIn Nanodroplets. *Langmuir* **33**, 9703–9710 (2017).

68. Zinkevich, M. & Aldinger, F. Thermodynamic Assessment of the Gallium-Oxygen System. *J. Am. Ceram. Soc.* **87**, 683–691 (2004).

69. Bartlett, M. D. & Majidi, C. High thermal conductivity in soft elastomers with elongated liquid metal inclusions - Supporting Information. *Proc. Natl. Acad. Sci.* 8–15 (2017) doi:10.1002/adma.201004109.

70. Finkenauer, L. R., Lu, Q., Hakem, I. F., Majidi, C. & Bockstaller, M. R. Analysis of the Efficiency of Surfactant-Mediated Stabilization Reactions of EGaIn Nanodroplets. *Langmuir* **33**, (2017).

71. Liu, S. *et al.* Can liquid metal flow in microchannels made of its own oxide skin? *Microfluid. Nanofluidics* **20**, 1–6 (2016).

72. Thompson, D. R., Rao, S. R. & Cola, B. A. A stepped-bar apparatus for thermal resistance measurements. *J. Electron. Packag.* **135**, 41002 (2013).

73. Ralphs, M. I., Smith, B. L. & Roberts, N. A. Technique for direct measurement of thermal conductivity of elastomers and a detailed uncertainty analysis. *Meas. Sci. Technol.* **27**, 115014 (2016).

74. Kempers, R., Kolodner, P., Lyons, A. & Robinson, A. J. A high-precision apparatus for the characterization of thermal interface materials. *Rev. Sci. Instrum.* **80**, 1–11 (2009).

75. Ralphs, M., Scheitlin, C., Wang, R. Y. & Rykaczewski, K. Buckling of Magnetically Formed Filler Fiber Columns Under Compression Increases Thermal Resistance of Soft Polymer Composites. *J. Heat Transfer* **141**, (2019).

76. He, Y. DSC and DMTA studies of a thermal interface material for packaging high speed microprocessors. *Thermochim. Acta* **392**, 13–21 (2002).

77. Koh, A., Sietins, J., Slipher, G. & Mrozek, R. Deformable liquid metal polymer composites with tunable electronic and mechanical properties. *J. Mater. Res.* **33**, 2443–2453 (2018).

78. Style, R. W., Tutika, R., Kim, J. Y. & Bartlett, M. D. Solid–liquid composites for soft multifunctional materials. *Adv. Funct. Mater.* **31**, 2005804 (2021).

79. Eshelby, J. D. The determination of the elastic field of an ellipsoidal inclusion, and related problems. *Proc. R. Soc. London. Ser. A. Math. Phys. Sci.* **241**, 376–396 (1957).

80. Palierne, J. F. Linear rheology of viscoelastic emulsions with interfacial tension. *Rheol. acta* **29**, 204–214 (1990).

81. Style, R. W. *et al.* Stiffening solids with liquid inclusions. *Nat. Phys.* **11**, 82–87 (2015).

82. Farrell, Z. J. & Tabor, C. E. Control of Gallium Oxide Growth on Liquid Metal Eutectic Gallium/Indium Nanoparticles via Thiolation. *Langmuir* **34**, 234–240 (2018).

83. Hayashi, Y., Saneie, N., Yip, G., Kim, Y. J. & Kim, J. H. Metallic nanoemulsion with galinstan for high heat-flux thermal management. *Int. J. Heat Mass Transf.* **101**, 1204–1216 (2016).

84. Zhang, W. *et al.* Liquid metal/metal oxide frameworks. *Adv. Funct. Mater.* **24**, 3799–3807 (2014).

85. Ren, L. *et al.* Nanodroplets for Stretchable Superconducting Circuits. *Adv. Funct.*

Mater. 1–8 (2016) doi:10.1002/adfm.201603427.

86. Yamaguchi, A., Mashima, Y. & Iyoda, T. Reversible size control of liquid-metal nanoparticles under ultrasonication. *Angew. Chemie - Int. Ed.* **54**, 12809–12813 (2015).

87. Uppal, A. *et al.* Pressure-activated thermal transport via oxide shell rupture in liquid metal capsule beds. *ACS Appl. Mater. Interfaces* **12(2)**, pp.2625-2633 (2019).

88. Dickey, M. D. *et al.* Eutectic gallium-indium (EGaIn): A liquid metal alloy for the formation of stable structures in microchannels at room temperature. *Adv. Funct. Mater.* **18**, 1097–1104 (2008).

89. Mercadé-Prieto, R. *et al.* Compression of elastic–perfectly plastic microcapsules using micromanipulation and finite element modelling: Determination of the yield stress. *Chem. Eng. Sci.* **66**, 1835–1843 (2011).

90. Mercadé-Prieto, R. *et al.* Determination of the elastic properties of single microcapsules using micromanipulation and finite element modeling. *Chem. Eng. Sci.* **66**, 2042–2049 (2011).

91. Prasher, R. S., Jim, S., Suzana, P., Paul, K. & Wang, J. Thermal Resistance of Particle Laden Polymeric Thermal Interface Materials . *J. Heat Transfer* **125**, 1170–1177 (2003).

92. Mei, S., Gao, Y., Deng, Z. & Liu, J. Thermally Conductive and Highly Electrically Resistive Grease Through Homogeneously Dispersing Liquid Metal Droplets Inside Methyl Silicone Oil. *J. Electron. Packag.* **136**, 011009 (2014).

93. Uppal, A., Kong, W., Rana, A., Wang, R. Y. & Rykaczewski, K. Enhancing Thermal Transport in Silicone Composites via Bridging Liquid Metal Fillers with Reactive Metal Co-Fillers and Matrix Viscosity Tuning. *ACS Appl. Mater. Interfaces* **13(36)**, pp.43348-43355 (2021).

94. Mazurek, P., Vudayagiri, S. & Skov, A. L. How to tailor flexible silicone elastomers with mechanical integrity: a tutorial review. *Chem. Soc. Rev.* **48**, 1448–1464 (2019).

95. Qi, D., Zhang, K., Tian, G., Jiang, B. & Huang, Y. Stretchable electronics based on PDMS substrates. *Adv. Mater.* **33**, 2003155 (2021).

96. Kosta, T., Krawietz, T. R. & Mares Jr, J. O. Sylgard 184 mixture and natural aging study via quasi-static compressive modulus. in *AIP Conference Proceedings* vol.

2272 40007 (AIP Publishing LLC, 2020).

97. Uppal, A. *et al.* Pressure-Activated Thermal Transport via Oxide Shell Rupture in Liquid Metal Capsule Beds. *ACS Appl. Mater. Interfaces* **12**, 2625–2633 (2020).

98. Goff, J., Sulaiman, S., Arkles, B. & Lewicki, J. P. Soft materials with recoverable shape factors from extreme distortion states. *Adv. Mater.* **28**, 2393–2398 (2016).

99. Mehra, N. *et al.* Thermal transport in polymeric materials and across composite interfaces. *Appl. Mater. Today* **12**, 92–130 (2018).

100. Standard, A. D5470. *Stand. test method Therm. Transm. Prop. Therm. Conduct. Electr. Insul. Mater. West Conshohocken, PA ASTM Int.* **D5470**, (2006).

101. Kong, W. *et al.* Oxide-Mediated Formation of Chemically Stable Tungsten-Liquid Metal Mixtures for Enhanced Thermal Interfaces. *Adv. Mater.* **31**, 1904309 (2019).

102. Jeong, S. H. *et al.* Mechanically Stretchable and Electrically Insulating Thermal Elastomer Composite by Liquid Alloy Droplet Embedment. *Sci. Rep.* **5**, 18257 (2015).

103. Zhang, Y. *et al.* Phase relations of the Ag–Ga–N system. *J. Alloys Compd.* **429**, 184–191 (2007).

APPENDIX A

SUPPORTING INFORMATION FOR CHAPTER 2

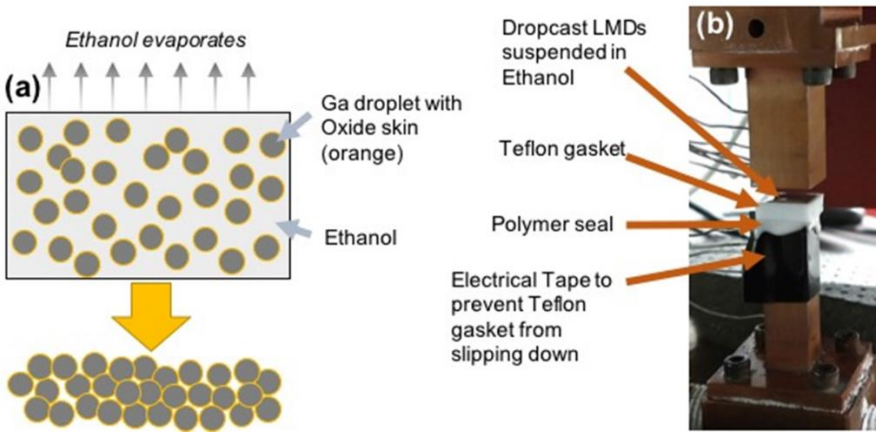

Figure A1: (a) Schematic illustrating drop casting of Ga LMDs, and (b) photograph of the SBA setup where the Ga LMDs are drop cased on the bottom bar[87]

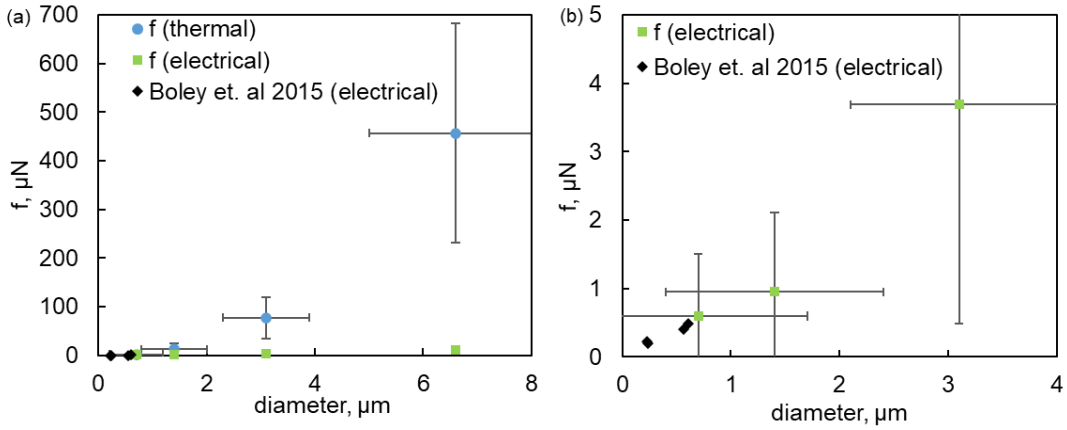

Figure A2: (a) Comparison of force per LM capsule required for rupturing the LM from Boley *et. al.*[64] with the experimental data of this work[87]

APPENDIX B

SUPPORTING INFORMATION FOR CHAPTER 3

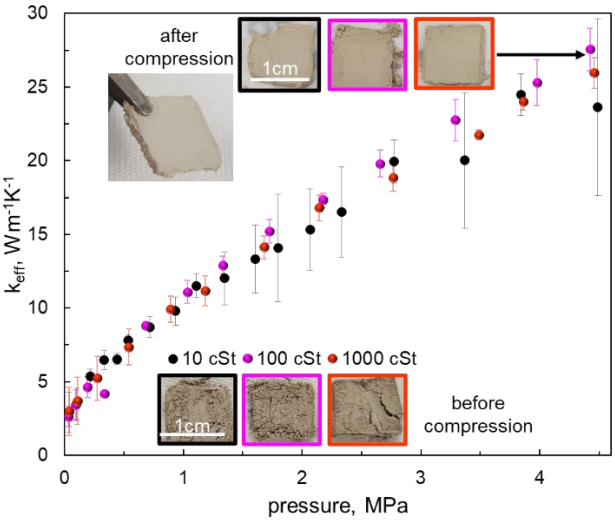

Figure B1: Impact of pressure on effective thermal conductivity of silicone oil-based composites with only silver solid metal fillers in 50 vol% silicone oil [93]

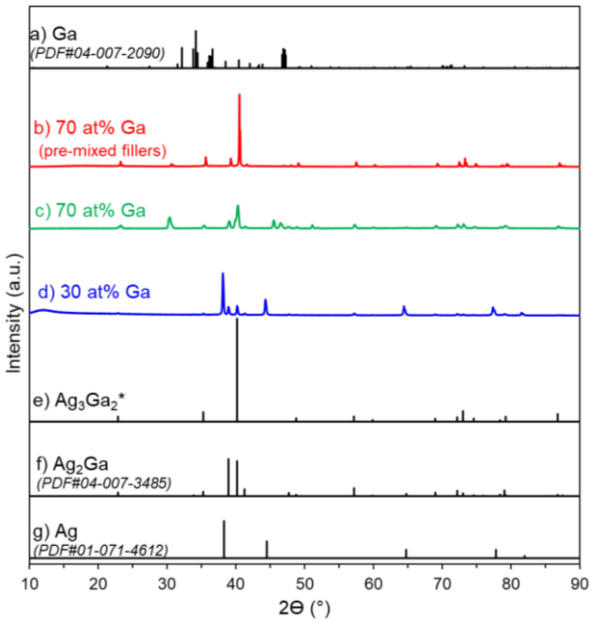

Figure B2: X-ray diffraction patterns of (a) Gallium powder diffraction file PDF# 04-007-2090; Ga-Ag-Silicone oil composites in 50 vol% 100cSt silicone oil at (b) 70 at% Ga with pre-mixed fillers, (c) 70 at% Ga, (d) 30 at% Ga; (e) Ag_3Ga_2* calculated diffraction pattern from Zhang et al.[103]; (f) Ag_2Ga diffraction file PDF# 04-007-3485and (g) Ag powder diffraction file PDF# 01-071-4612.

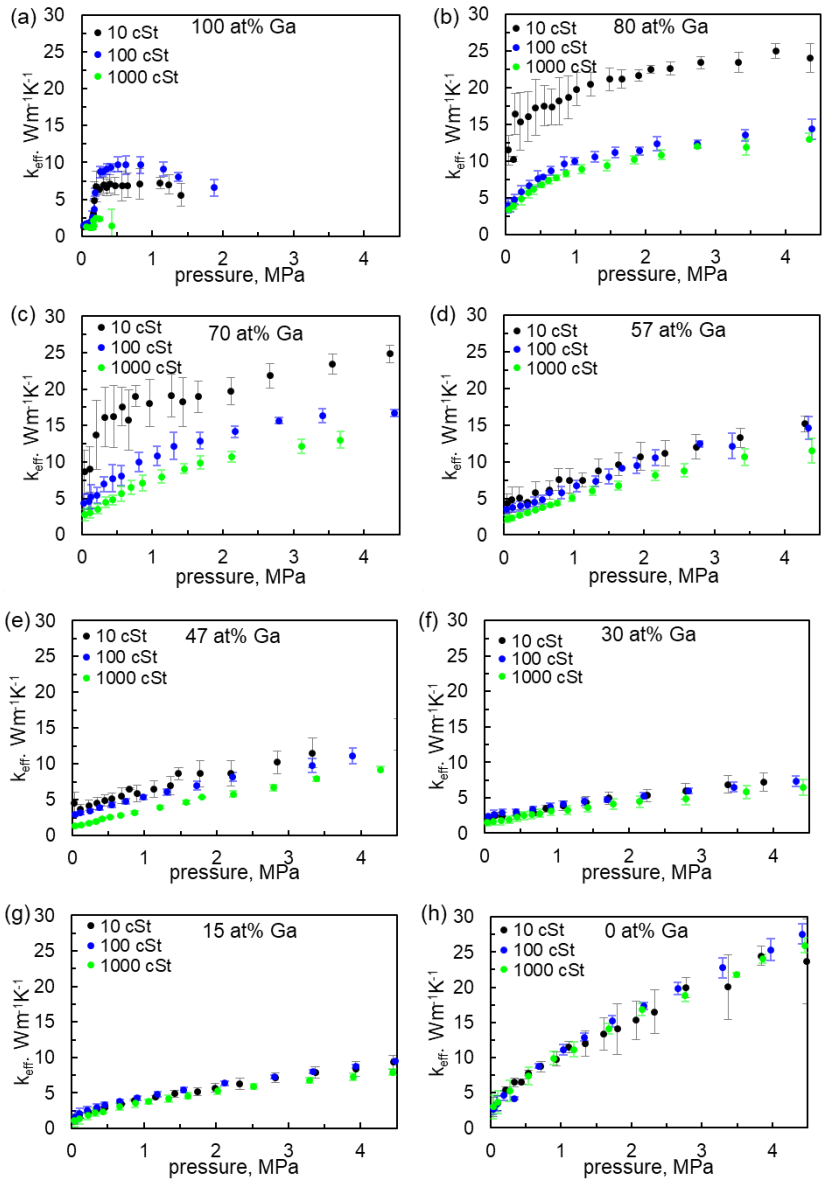

Figure B3: Variation of effective thermal conductivity with pressure for LM:Ag:silicone oil composites containing 50% volume oil with varying oil viscosity and filler fraction of (a) 100 at% Ga, (b) 80 at% Ga, (c) 70 at% Ga, (d) 57 at% Ga, (e) 47 at% Ga, (f) 30 at% Ga, (g) 15 at% Ga and (h) 0 at% Ga.

APPENDIX C

SUPPORTING INFORMATION FOR CHAPTER 4

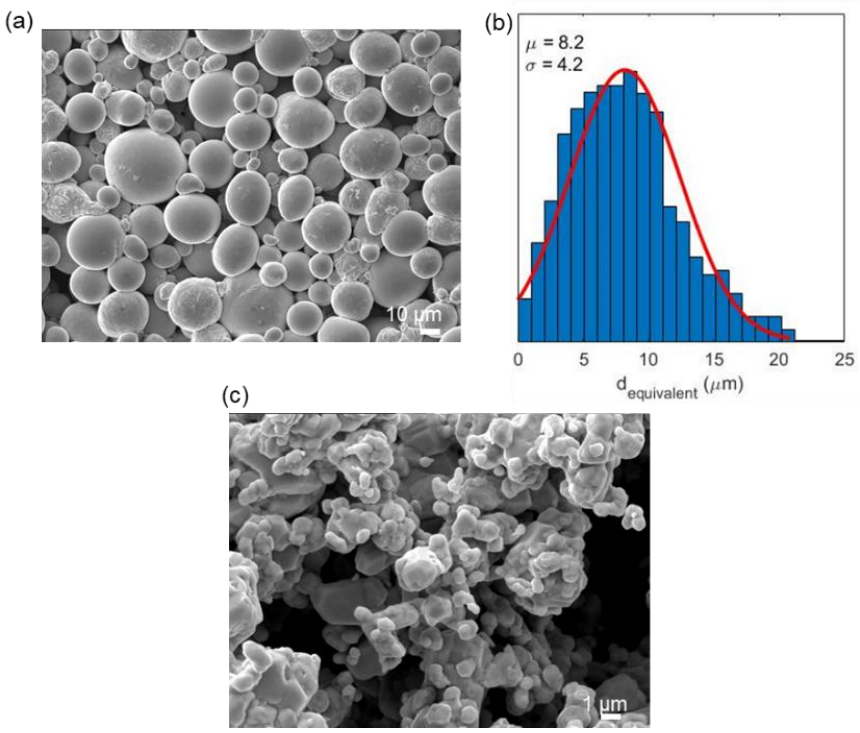

Figure C1: (a) SEM image of fabricated Ga droplets, (b) Ga particle size distribution, and (c) SEM image of the commericially-acquired Ag particles used in the work (Alfa Aesar, APS 4-7 μm particle size)

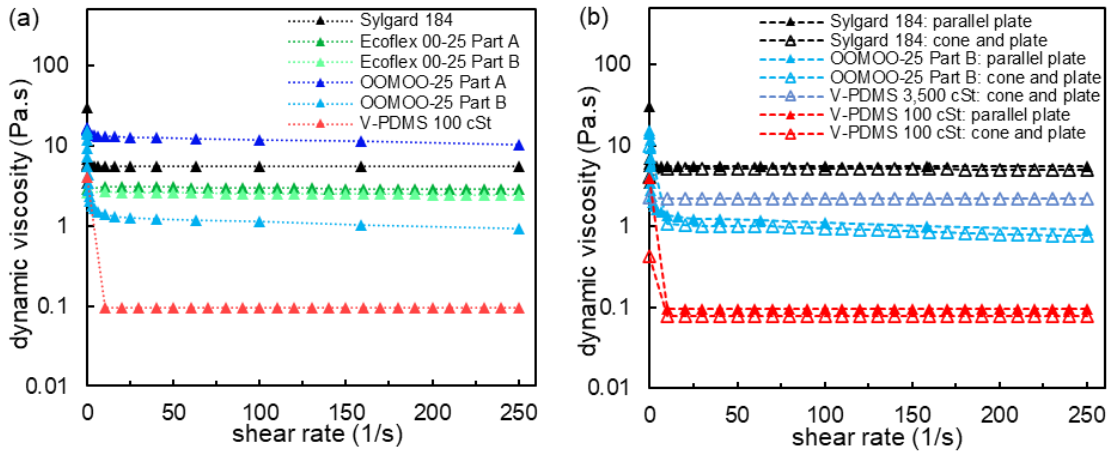

Figure C2: (a) Rheological behavior of the three commercial silicone kits: Sylgard 184, Ecoflex 00-25, OOMOO-25, and the tailor-made formulation of V-PDMS 100 cSt formulation using parallel plate geometry (ϕ25 mm) and, (b) dynamic viscosity using cone-and-plate geometry (ϕ20 mm, cone angle 1.995°) for Sylgard 184, OOMOO-25 part "B", V-PDMS 100 cSt and 3,500 cSt formulation.

Table C1: (a) Measured viscosity of individual components of commercial elastomer kits, and (b) Comparison of measured viscosity with reported values in the material technical datasheet.

(a)

Pre-cursor component	**Measured viscosity** (parallel plate geometry)
Ecoflex 00-20 part "A"	2.9 Pa.s
Ecoflex 00-20 part "B"	2.5 Pa.s
OOMOO-25 part "A"	11.4 Pa.s
OOMOO-25 part "B"	1.1 Pa.s 0.78 Pa.s (cone-and-plate geometry)

(b)

Silicone elastomers	**Density**	**Technical data sheet viscosity**	**Measured viscosity**	
			Parallel plate geometry	Cone and plate geometry
Sylgard 184	1.03 gml^{-1}	4-5.5 Pa.s	5.5 Pa.s ***(5340 cSt)***	5.1 Pa.s ***(4951 cSt)***
Ecoflex 00-20	1.07 gml^{-1}	3.0 Pa.s	2.7 Pa.s ***(2523 cSt)***	-
OOMOO-25	1.34 gml^{-1}	4.25 Pa.s	5.0 Pa.s ***(3731 cSt)***	-
V-PDMS (100 cSt formulation)	0.97 gml^{-1}		0.096 Pa.s ***(99 cSt)***	0.078 Pa.s ***(80 cSt)***
V-PDMS (3,500 cSt formulation)	0.97 gml^{-1}		-	2.2 Pa.s ***(2268 cSt)***

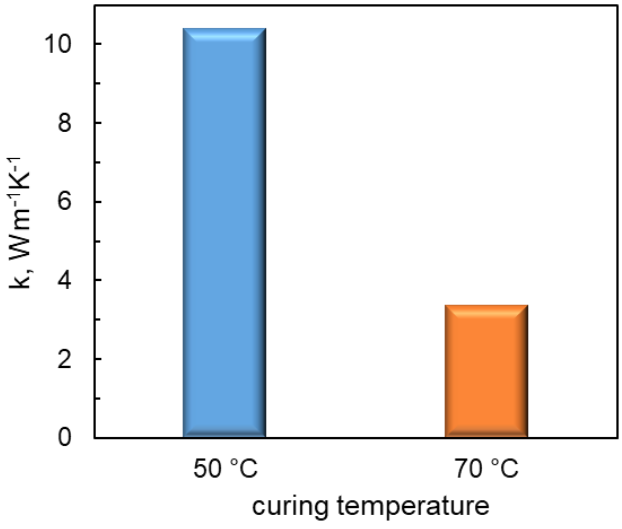

100 cSt based polymer pad
37:13:50 Ga:Ag:V-PDMS v/v
0.8 MPa curing pressure

Figure C3: Variation of thermal conductivity with curing temperature

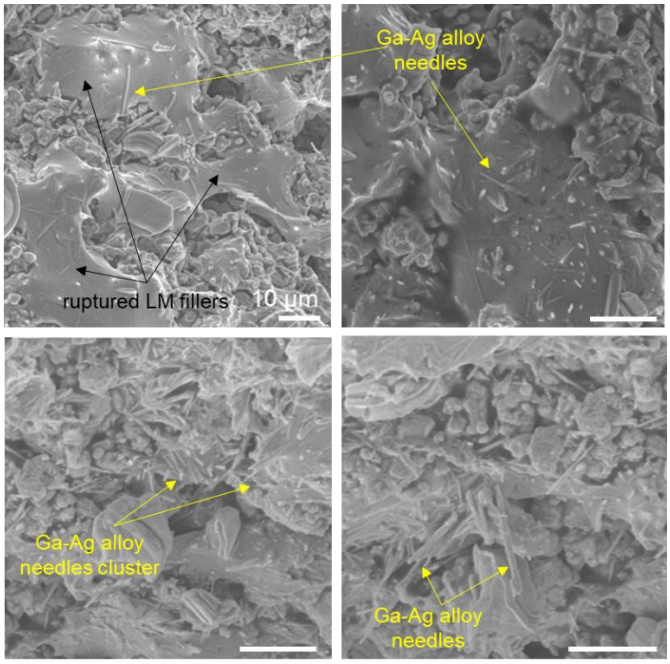

Figure C4: Illustrative electron micrographs of liquid metal-silver alloy needles present in composite pads made with the 100 cSt V-PDMS formation.

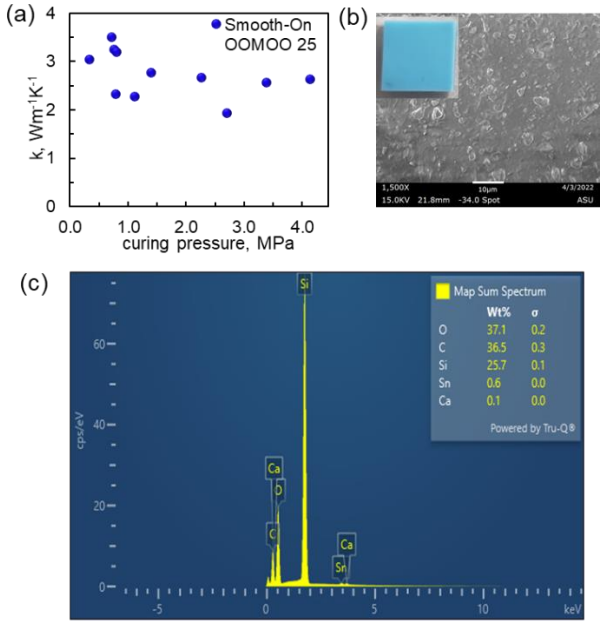

Figure C5: (a) Thermal conductivity of OOMOO-25 silicone with gallium and silver fillers (50 vol% functional fillers, 70 at% Ga), (b) SEM of OOMOO-25 pad with no fillers added during fabrication of pads (100 vol% OOMOO-25 polymer), and (c) Energy-dispersive spectroscopy (EDS) element graph of an OOMOO-25 polymer pad with no fillers added during fabrication of pads.

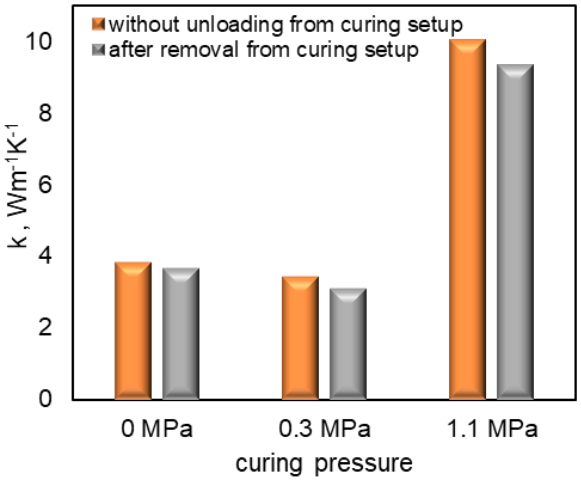

Figure C6: Thermal conductivity of cured pads (37:13:50 v/v Ga:Ag:V-PDMS$_{100\ cSt}$) as samples are re-measured at 0.2 MPa measurement pressure after removal from the curing setup

BIOGRAPHICAL SKETCH

Aastha Uppal was born in 1990 in India and grew up there. She completed her high school and undergraduate studies in India, where she attended University of Pune to get her Bachelor of Engineering in Mechanical Engineering in 2012. She then accepted a position in Tata Motors, where she worked as an Assistant Manager in the Power Train manufacturing assembly line of automobiles. After 2 years of working in the automotive industry, she moved to the United States in 2014 to pursue her Master of Science in Mechanical Engineering from Arizona State University. She graduated in May 2016 with a Thesis titled “Development of Breathable, Self-Sealing Protective Garment” under Dr. Konrad Rykaczewski. She then accepted a position as Packaging R&D Engineer at Intel Corporation in Chandler, Arizona, where she continues to work full-time. She started her Ph.D. in August 2018 while working full-time with full tuition assistance from Intel. She was co-advised by Dr. Konrad Rykaczewski and Dr. Robert Wang and will graduate with her Ph.D. in Mechanical Engineering in December 2022. She is continuing her full-time job with Intel in Chandler, Arizona, after completing her Ph.D.